Paleoceanography and Paleoclimatology

RESEARCH ARTICLE
10.1029/2020PA004175

Key Points:

- Coccolithophore ε_p sensitivity to CO_2[aq] is consistent with that observed in cultures but contrasts with predictions of classical diffusive models of CO_2 acquisition
- Geochemical, micropaleontological, and morphometrical proxies are assessed as indicators of the non-CO_2 effects on ε_p
- *Gephyrocapsa* coccoliths show coupled variations in oxygen and carbon isotope vital effects over the time series

Supporting Information:

Supporting Information may be found in the online version of this article.

Correspondence to:

A. González-Lanchas,
lanchas@usal.es

Citation:

González-Lanchas, A., Hernández-Alméida, I., Flores, J.-A., Sierro, F. J., Guitian, J., & Stoll, H. M. (2021). Carbon isotopic fractionation of alkenones and *Gephyrocapsa* coccoliths over the Late Quaternary (marine isotope stages 12–9) glacial-interglacial cycles at the western tropical Atlantic. *Paleoceanography and Paleoclimatology*, *36*, e2020PA004175. https://doi.org/10.1029/2020PA004175

Received 9 DEC 2020
Accepted 5 JUL 2021

Carbon Isotopic Fractionation of Alkenones and *Gephyrocapsa* Coccoliths Over the Late Quaternary (Marine Isotope Stages 12–9) Glacial-Interglacial Cycles at the Western Tropical Atlantic

A. González-Lanchas[1], I. Hernández-Alméida[2], J.-A. Flores[1], F. J. Sierro[1], J. Guitian[2], and H. M. Stoll[2]

[1]Departamento de Geología, Universidad de Salamanca, Salamanca, Spain, [2]Geological Institute, ETH Zürich, Zürich, Switzerland

Abstract The sensitivity of coccolithophores to changing CO_2 and its role modulating cellular photosynthetic carbon isotopic fractionation (ε_p) is crucial to understand the future adaptation of these organisms to higher CO_2 world and to assess the reliability of ε_p for past CO_2 estimation. Here, we present ε_p measured on natural fossil samples across the glacial-interglacial (G-I) CO_2 variations of marine isotope stages 12 to 9 interval (454–334 ka) at the western tropical Atlantic Ocean Drilling Program Site 925 together with a set of organic and inorganic geochemical, micropaleontological and morphometrical data from *Gephyrocapsa* coccoliths in the same samples. The ~2‰ variation in ε_p is significantly correlated with the CO_2[aq] concentrations calculated from assumption of air-sea equilibrium with measured ice core pCO_2 concentrations. The sensitivity of ε_p to CO_2[aq] is similar to that derived from a multiple regression model of culture observations and is not well simulated with the classical purely diffusive model of algal CO_2 acquisition. The measured range of *Gephyrocapsa* cell sizes is insufficient to explain the non-CO_2 effects on ε_p at this location, via either direct size effect or growth rate correlated to cell size. Primary productivity, potentially triggered by shifting growth rates and light levels, may also affect ε_p. Proposed productivity proxies % *Florisphaera profunda* and the ratio between the C_{37} to $C_{38.et}$ alkenone (C37/C38.et ratio) both correlates modestly with the non-CO_2 effects on ε_p. When the observed G-I ε_p to CO_2 sensitivity at this site is used to estimate pCO_2 from ε_p since the Miocene, the inferred pCO_2 declines are larger in amplitude compared to that calculated from a theoretical ε_p diffusive model. We find that oxygen and carbon stable isotope vital effects in the near monogeneric-separated *Gephyrocapsa* coccoliths (respectively $\Delta\delta^{18}O_{Gephyrocapsa-Trilobatus\ sacculifer}$ and $\varepsilon_{coccolith}$) are coupled through the time series, but the origins of these vital effects are not readily explained by existing models.

1. Introduction

Coccolithophores, single-celled marine phytoplankton, play a unique role in the marine carbon cycle because their primary production contributes to both the operation of the carbonate counter pump and the biological organic carbon pump during their lifecycle. There is considerable interest in understanding their past role in the carbon cycle and how their growth and calcification may have been affected by changing oceanographic conditions and changing CO_2 availability (e.g., Bach et al., 2011, 2013; Rigual-Hernández et al., 2020).

At the same time, they produce alkenones, organic biomarkers preserved in sediments, which have been widely applied for two proxies: (a) using the unsaturation ratio of C_{37} ketones $\left(U^{k'}_{37}\right)$, as a proxy for temperature (Müller et al., 1998; Prahl & Wakeham, 1987) and (b) using the photosynthetic carbon isotopic fractionation of alkenones (ε_p), to estimate past changes in carbon limitation of algae as an indicator of changing pCO_2 (e.g., Pagani et al., 1999, 2011; Seki et al., 2010; Y. G. Zhang et al., 2013).

In addition, the carbon and oxygen isotopic composition of their intracellularly produced coccoliths (calcite platelets) are being explored to evaluate if they might provide additional paleoclimatic information. Early studies (e.g., Dudley et al., 1986; Ziveri et al., 2003) documented that the coccolith isotopic composition did not reflect equilibrium precipitation from seawater but was offset due to "vital effects." Recent models

(Bolton & Stoll, 2013; Hermoso et al., 2014; Holtz et al., 2017; McClelland et al., 2017; Ziveri et al., 2012) have explored whether such vital effects might record different aspects of coccolithophore physiology during cellular growth, such as the ratio of calcification to photosynthesis, carbon uptake and allocation strategies or changes in the dissolved (aqueous) seawater concentration of CO_2 (hereafter referred as CO_2[aq]).

While the alkenone temperature proxy is widely applied as a standard temperature indicator, many open questions remain regarding the application of ε_p for pCO_2 estimation. The ε_p is expected to increase with a higher CO_2 supply to photosynthesis relative to the cellular carbon demand (see Pagani, 2014 for a review). Traditionally, this dependence has been modeled as a passive cellular CO_2 acquisition by diffusive transport, in which ε_p varies as a function of CO_2[aq] and the physiological parameter b (Bidigare et al., 1997; Rau et al., 1996). According to the physical diffusive model, b is most sensitive to cell size, algal growth rate and the cell permeability to CO_2[aq]; whereas abiotic factors such as ocean temperature, pH and salinity only exert a minor influence on b (Bidigare et al., 1997). Under the perspective of this classical model, the limited variation in ε_p over known quaternary glacial-interglacial (G-I) variations in pCO_2 has led some to question the suitability of ε_p as a pCO_2 proxy (see Badger et al., 2019). Recent aggregate analysis of a large experimental culture data set suggest that the ε_p dependence on CO_2 does not follow a purely diffusive model, and that similarly, ε_p is less sensitive to glacial CO_2 variations in some sites than predicted by this classical approach (Stoll et al., 2019). One explanation is that intracellular active carbon transport systems sustain carbon concentrating mechanisms (CCM; Cassar et al., 2006; Laws et al., 2002), resulting in the observed lowered sensitivity of ε_p to CO_2 within the low CO_2 range. Among recent contributions considering the role of CCM on ε_p for pCO_2 reconstruction, Badger (2021) suggested a 7 μmol L^{-1} threshold for the operation of the CCM, proposing the breakdown of the diffusive alkenone pCO_2 approach below this threshold concentration. The culture-based regression of the ε_p dependence on CO_2[aq] by Stoll et al. (2019) incorporates the operation of these non-diffusive mechanisms, regardless of the existence of a threshold, and offers the opportunity to evaluate the implication of further reconstructed coccolithophore physiological (i.e., cell size and growth rate) and environmental (i.e., light) constrains affecting ε_p.

The most important physiological and environmental processes contributing to carbon and oxygen isotope vital effects in coccoliths remain under investigation. Coccolith oxygen isotopic vital effects have been proposed to reflect the intracellular pH of the calcification space due to the pH effect on the relative contribution of the different carbonate species to calcification (e.g., Langer et al., 2006; Ziveri et al., 2012). This mechanism is analogous to that proposed in planktic foraminifera (e.g., Zeebe, 1999) and arises because of varying fractionation factors between water and the different dissolved carbon species. Alternatively, changes in the intracellular residence time of dissolved carbon species related to cellular growth rates was proposed to regulate oxygen isotope vital effects (e.g., Hermoso et al., 2014). Carbon isotopic fractionation of coccoliths is modeled to be controlled by several factors, such as intracellular HCO_3^- allocation between photosynthesis and calcification, the significance of HCO_3^- pumping into the cell, CO_2[aq], organic carbon fixation rate, and the calcification/photosynthesis ratio (e.g., Bolton & Stoll, 2013; Holtz et al., 2017; McClelland et al., 2017), but experimental confirmation of these processes in culture studies remains sparse, and only few studies have explored the effects in coccoliths produced in the ocean under known CO_2 conditions, as reviewed in Stoll et al. (2019).

In this contribution, we explore the processes influencing the variations in ε_p and vital effects in *Gephyrocapsa* coccolith carbon and oxygen isotopes in natural samples recovered from sediments from the Western Tropical Atlantic (WTA) warm pool between the Marine Isotope Stage (MIS) 12 to MIS 9 (454–334 ka). The low amplitude of the eccentricity changes during this interval (e.g., Jansen et al., 1986) minimizes the effect of the variance in the magnitude of precessional forcing on productivity and potentially growth rate, increasing the signal/noise ratio for the main research question in this study: the relationship between ε_p and CO_2. This period contains, furthermore, strong contrasts from the extreme glacial MIS 12 to the longest interglacial MIS 11(e.g., Lang & Wolff, 2011; Yin & Berger, 2012), that provides a broad spectrum to test our results under high and low CO_2 endmembers during the late Quaternary. A conspicuous feature of this interval is the dominance of the *Gephyrocapsa* genus in the global ocean (Baumann & Freitag, 2004; Bollmann et al., 1998), the main coccolithophore alkenone producer prior to the appearance and proliferation of *Emiliania huxleyi* at ~280 ka (e.g., Volkman, 2000). As a result, coccolith assemblages in sediment records are nearly monogeneric, facilitating the generation of coccolith geochemical records derived from

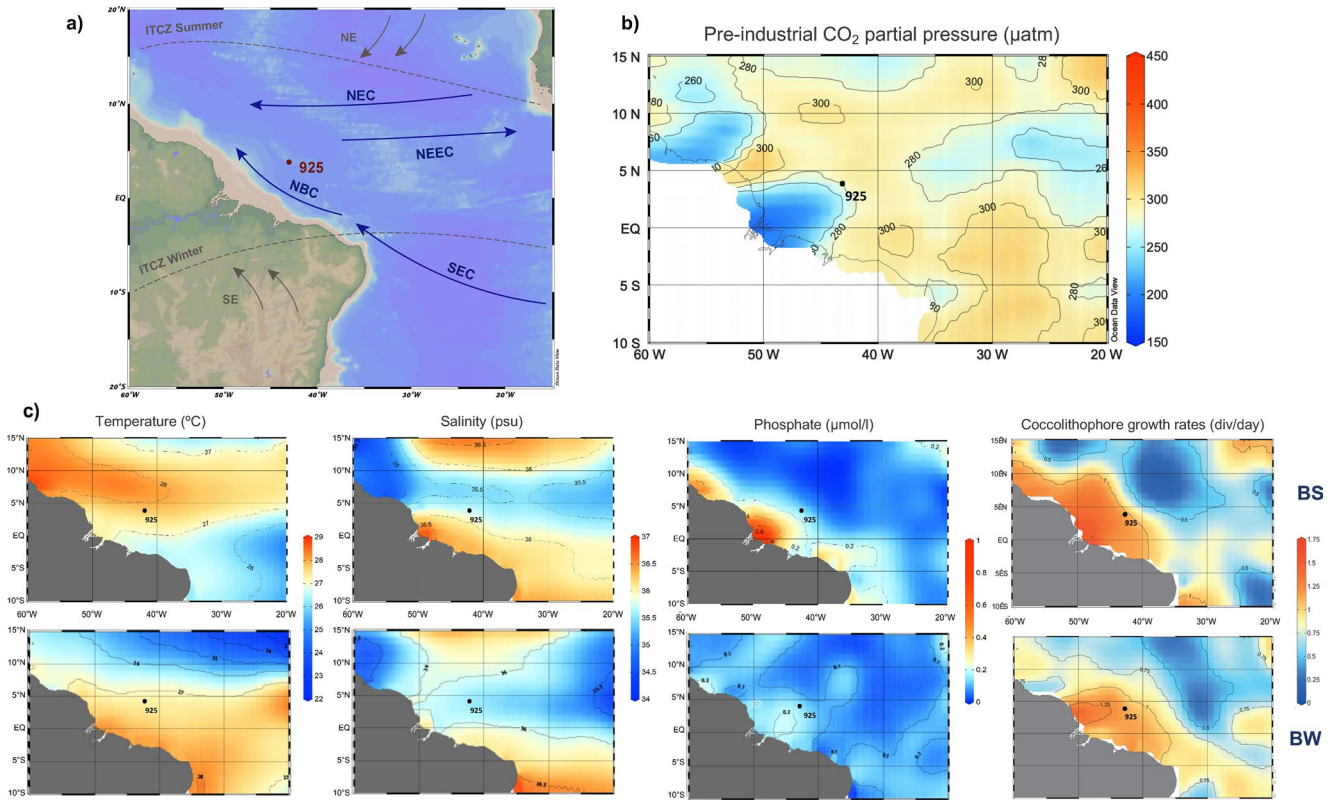

Figure 1. (a) Geographic location of the ODP Site 925 and modern oceanographic and climatic scheme. Arrows indicates the trajectories of water masses (in blue) and wind systems (in gray). North Equatorial Current; North Equatorial Counter Current; North Brazilian Current; South Equatorial Current; and Intertropical Convergence Zone. (b) Pre-industrial CO_2 partial pressure (µatm) in the regional ocean surface calculated with MOCSY 2.0 (Orr & Epitalon, 2015) using SST and salinity from GLODAP (Olsen et al., 2016; Key et al., 2015). (c) Seasonal variability at 10 m depth of temperature (°C), salinity (psu), phosphate concentration (µmol l^{-1}), and coccolithophore growth rate (divisions day^{-1}; Krumhardt et al., 2017). Temperatures, salinities, and [PO_4^{3-}] were extracted from the Locarnini et al. (2013) and were plotted using Ocean Data View (Schlitzer, 2008). BS, Boreal summer; BW, Boreal winter.

few closely related *Gephyrocapsa* species (e.g., Bendif et al., 2019), and assessing a unique haptophyte group as alkenone source.

The ODP Site 925 has been previously selected for the reconstruction of CO_2, using both boron isotope (Foster et al., 2012; Sosdian et al., 2018) and the alkenone pCO_2 proxy, including the longest single site pCO_2 record from present to 40 my (Y. G. Zhang et al., 2013). This site has been chosen for these studies because it is not affected by upwelling and sufficiently distant from coastal influences, so that it is interpreted to have remained close to equilibrium with atmospheric CO_2. It maintains very low (<18 µatm) post-industrial air-sea pCO_2 difference (Takahashi et al., 2009) and a low air-sea disequilibrium in the pre-industrial (Figure 1b). It has been, as well, considered for the study of long term evolution of coccolithophore stable isotope vital effects and cellular calcification (e.g., Bolton et al., 2016). In general, tropical sites offer some advantages for the study of the effect of varying CO_2[aq] on coccolithophore proxies: temperature changes are lower than high latitude locations because they are much less affected by the G-I movements of the polar fronts (e.g., Rehfeld et al., 2018), so pCO_2 is the main driver of CO_2[aq] variations. However, at the location of Site 925, there is only limited published data of ε_p and coccolith stable isotope fractionation during a quaternary G-I (e.g., Stoll et al., 2019; Y. G. Zhang et al., 2013) to evaluate these proxies against independently constrained variations in pCO_2 from available ice core records.

We therefore provide new determinations of ε_p from biomarker analyses and new determinations of carbon and oxygen vital effects from separated coccoliths of the genus *Gephyrocapsa*; hence, we provide matched records of the organic and inorganic carbon isotopic fractionation in coccoliths. The sea surface temperature (SST) and productivity conditions are well reconstructed from $U^{k'}_{37}$ index, the $\delta^{18}O$ gradients between surface and intermediate dwelling planktic foraminifera species, coccolith counts, *% Florisphaera profunda*

and the ratio between the C_{37} to $C_{38.et}$ alkenone (C37/C38.et ratio). *Gephyrocapsa* coccolith morphometry (coccolith length, mass, and thickness) and coccolith assemblage characterization provide additional information on the production environment and surface ocean conditions. The integration of all of these proxies gives us a unique opportunity to parse out the effect of the changing environmental conditions at the WTA and the physiological modulation from *Gephyrocapsa* on ε_p across the investigated period. Specifically, we are able to compare the new ε_p observations with the predictions of the diffusive and culture-derived models of the relationship between ε_p and CO_2[aq]. In addition, we evaluate whether other independent proxies have power to predict the non-CO_2 influences on ε_p

2. Modern Oceanographic Setting of the Western Tropical Atlantic

The studied ODP Site 925 (4°12.249′N; 43°29.334′W) is located in Ceara Rise, the western sector of the tropical Atlantic Ocean (WTA; Figure 1a). Surface circulation in the region is characterized by the preferential westward flow of the North Equatorial Current (NEC; Figure 1a). South of the NEC, the North Equatorial Counter Current (NEEC; Figure 1a), flows in a counter direction (Stramma & Schott, 1999). The North Brazilian Current (NBC; Figure 1a) is the northward bifurcation of the South Equatorial Current (SEC; Peterson & Stramma, 1991).

The seasonal variability in surface ocean conditions is driven by the seasonal shifts in the intensities of SE and NE trade winds and the coupled migration of the Intertropical Convergence Zone (ITCZ; Figure 1a). During boreal summer and fall, the strengthening of SE trade wind system promotes the northernmost movement of the ITCZ and intensification of the westward circulation. In turn, this is the time of NECC development (Hastenrath & Merle, 1987). The NBC experiments a detachment from its Brazilian-coast pathway and retroflects eastward into the NEEC (Richardson & Reverdin, 1987). Most of the Amazon discharges concentrate in the shelf, but 7%–17% of terrigenous particles are transported northwest through NBC as dispersion plumes. During boreal winter and spring, when the NE trade winds intensify, the ITCZ reach it southwardmost position (Figure 1a). This causes the disappearance of the NECC. At this time, the NBC continues to flow north-westward off the South American coasts (Philander, 2001; Richardson & Reverdin, 1987).

In the modern WTA, the depth of the mixed layer is stable, with near-permanent highly stratified surface conditions through the entire year (Philander & Pacanowski, 1986). A strong thermocline and nutricline below the photic zone (>100 m) limits the nutrient renewal and the primary productivity in the upper photic zone (see Mann & Lazier, 2006). Surface temperatures and salinities are high and stable throughout the year, with a small temperature increase during the summer (Figure 1c; Locarnini et al., 2013) most likely related to the slight thermocline deepening by pileup of SEC waters (Hastenrath & Merle, 1987). As light and temperature are not limiting factors in the region, changes in coccolithophore growth and production rates are controlled by the changes in nutrient distribution through the euphotic zone (Kinkel et al., 2000). Surface phosphate concentrations and coccolithophore growth rates seasonally range around 0.1–0.2 $\mu mol\ l^{-1}$ (Locarnini et al., 2013) and 1–1.25 day^{-1} (Krumhardt et al., 2017), respectively, with slight increases during the summer (Figure 1c). Despite modest changes, coccolithophore fluxes are highest during the summer and fall, when the water column is stabilized by the northward positioning of ITCZ and weaker influence of NE trades (Guerreiro et al., 2017). Minima in coccolithophore fluxes were found during winter and spring, associated with water column instabilities due to the southward displacement of ITCZ and intensified influence of NE trade winds (Guerreiro et al., 2017).

As important feature in the modern setting, significant stimulation of coccolithophore primary productivity is driven by the eventual nutrient input of Amazon origin (Korte et al., 2020). Higher fluxes of opportunistic species like *Emiliania huxleyi* and those belonging to the *Gephyrocapsa* genus were consistently described as fast productivity response to the increased input of low-salinity and nutrient-enriched waters within the upper ~50 m (e.g., Demaster & Pope, 1996; Guerreiro et al., 2017).

3. Sediments and Inference of pCO_2 for Sampled Intervals

The studied materials were retrieved during the expedition ODP 154. The ODP Site 925 is located at 3.040 m water depth, in the shallowest part of Ceara Rise, well above the modern carbonate lysocline (at 4.500 m; Bickert et al., 1997). The studied interval, from 12.96 to 18.80 mcd (meters composite depth) of the splice, corresponds to holes B and C. Sediments are characterized by a continuous alternation of nannofossil clay and nannofossil ooze (Curry et al., 1995).

Twelve samples were selected following the available age model by Wilkens et al. (2017), covering the interval between MIS 12 to MIS 10/MIS 9 (454.24–334.69 ka).

A critical step is the proper assignment of a reference ice core pCO_2 value for each of the samples considered in this study. To minimize uncertainty due to absolute chronology in both the marine record and Antarctic ice cores, the pCO_2 corresponding to each sample age was derived from the regression between the deep North Atlantic $\delta^{18}O$ benthic stack LS16 (Lisiecki & Stern, 2016) and the pCO_2 ice core compilation by Köhler et al. (2017) for the last 40 kyr, which is constrained by ^{14}C dates in the marine archive and layer counted Antarctic ice core chronology back to 30 ka. Results and calibration are shown in Text S1 and Figures S1 and S2. The corresponding CO_2[aq] values for our samples are calculated using Henry's law. We use the alkenone-derived SST at Site 925 for the calculation of CO_2 solubility. Detailed information and the conversion of values from pCO_2 to CO_2[aq] for each sample is included in Text S1 and Table S1.

4. Analytical Methods and Calculations

4.1. Alkenone Analysis and Proxies

Lipids were extracted from 20 g freeze-dried sediment at ETH Zürich with the use of an *Accelerated Solvent Extraction 350*. The lipids were saponified using ~2 ml of a 0.5 M solution of potassium hydroxide (KOH) in 95:5 methanol (MeOH)/H_2O and the neutral fraction extracted with hexane (C_6H_4). The hydrocarbon, ketone and polar organic fractions were separated through silica gel columns, respectively eluted with 4 ml of C_6H_4, dichloromethane (CH_2C_2), and MeOH. The ketone quantification was carried out on a *Thermo Scientific Trace 1310 Gas Chromatograph* (GC) coupled to a Flame Ionization Detector (FID). GC-FID was equipped with an Agilent capillary column (60 m × 0.25 mm × 0.25 μm) *VF – 200 ms* and a 5-m guard column. Helium (He) at 2 ml min^{-1} was used as carrier gas flow. GC oven was set at 60°C for a minute after injection and then ramped at 20°C min^{-1} to 255°C, 3°C min^{-1} to 300°C, and finally 10°C min^{-1} to 320°C to be held 5 min.

The $U^{k'}_{37}$ index (Brassell et al., 1986) was calculated after the abundance of the C_{37} di- and triunsaturated ketones. C_{39} *n*-alkane was added to every sample as internal standard, and replicates and an in-house alkenone standard was injected at every sequence to determine the analytical accuracy of 0.025 $U^{k'}_{37}$ units. The $U^{k'}_{37}$ index was converted into SST values with the BAYSPLINE calibration (Tierney & Tingley, 2018), which re-examined available core top data and improves the attenuation observed at high $U^{k'}_{37}$ with classical linear calibrations, producing a better fit for the SST changes in tropical regions.

Following the connection between the ratio of production of C_{37} to C_{38} organic compounds with haptophyte growth rates proposed by Herbert et al. (2018), the proportion of C_{37} to $C_{38.et}$ (C37/C38.et) was calculated; it was proposed that the increase in the value of this ratio implies an increase in the growth rate of the producers that, in this case, corresponds to *Gephyrocapsa*.

The carbon isotopic composition of the diunsaturated alkenone $C_{37:2}$ (δ^{13} $C_{37:2}$) was analyzed on a Delta V isotope-ratio mass spectrometer coupled to a *Trace 1310 GC* (GC-IRMS) from *Thermo Scientific* at ETH Zürich. Combustion reactor was oxidized for one hour and seed oxidized during one minute before each sequence and injection respectively with equivalent purge of He backflush time. GC was equipped as the GC-FID previously described. Oven temperature was set at 90°C for injection to be ramped after 1 min to 250°C at 25°C min^{-1}, 1°C min^{-1} to 305°C, and finally to 320°C at 10°C min^{-1}. The, temperature was kept isothermal for 10 min. To determine analytical precision of the measurements, molecular standards A6 and B4, containing *n*-alkanes of known isotopic mixtures (supplied by Arndt Schimmelmann, University of Indiana) replicates and an in-house standard were injected in every sequence to determine the analytical

accuracy. Values are reported relative to the Vienna Pee Dee Belemnite (VPDB) standard. Measurement replicates yielded a mean difference of 0.5‰.

4.2. Planktic Foraminifers

Bulk samples were sieved through 425, 350, 250 and 150 μm with DI water and oven dried overnight at 50°C. Foraminifers where picked from narrow size ranges to minimize large changes in the isotope signal due to size variations (Ezard et al., 2015). Approximately, 15 specimens of *Neogloboquadrina dutertrei* were extracted from the 425–350 μm fraction and the same number of specimens of *Trilobatus sacculifer* (without sac, var. *Trilobatus inmaturus*; Leroy, 1939) and *Globigerinoides ruber* ("white" sensu stricto; Aurahs et al., 2011) from the 350–250 μm fraction. The foraminifer specimens were crushed with two clean moistened glass-slides and rinsed two times in ultrapure MilliQ water. After adding 500 μl of methanol, samples were ultrasonicated for 1 min. Clays were removed with a pipet as an overlying residue. The remaining carbonate content was oven dried overnight at 50°C. Stable isotope analyses were carried out at ETH Zurich (see Section 4.4. for further instrumental details).

The selected species *G. ruber* and *T. sacculifer* dwell near the surface, from 0 to 50 m (Ravelo & Fairbanks, 1992), while *N. dutertrei* is a common thermocline dweller, between 60 and 150 m (Steph et al., 2009). A foraminifer multispecies isotopic approach allows to trace the physical and chemical structure of the mixed layer and thermocline across during the interval. To correct for the influence of species-specific fractionation factors on oxygen isotopes, we applied the species-specific normalization values at 25°C summarized by Spero et al. (2003) to the measured isotope values (Figure 2c). For $\delta^{18}O$, these normalization factors are derived from empirical culture or plankton tow regressions of temperature and foraminiferal $\delta^{18}O$ and normalize the other species to the *G. ruber* calibration; that is, we apply the correction factors of –0.11‰ and +0.05‰, respectively to *T. sacculifer* and *N. dutertrei* (see Spero et al., 2003 and references therein).

4.3. *Gephyrocapsa* Coccolith Microfiltration

The coccolith assemblages were extracted and size-separated to isolate the fraction containing the species belonging to the *Gephyrocapsa* genus (see Text S3). An amount of 0.5 g of bulk sample was disaggregated by suspension in 2% ammonia solution and ultrasonication. Larger-sized particles were removed by filtering through a 20 μm nylon mesh. The <2 μm fraction, which includes *Florisphaera profunda,* was removed on the basis of its slow settling velocity (H. Zhang et al., 2018). Subsequently, we used 5 and 3 μm polycarbonate membranes to filter a 2 L suspension of the sediment in 2% ammonia to produce a 3–5 μm coccolith fraction. Size fractions were collected by high-speed (4000 RPM) centrifugation, and pellets were rinsed with ultrapure water (Milli-Q). After removing the liquid with a pipette, the coccolith fractions were oven-dried overnight at 50°.

The separation efficiency was checked in smear slides and confirmed that the 3–5 μm fraction is dominated by the *Gephyrocapsa* genus with an average proportion of 86.6%. The <3 μm fraction, which also contains *Gephyrocapsa* individuals of 2–3 μm, was not further analyzed as it contained a proportion of undetermined small carbonate fragments.

4.4. Stable Isotope Analysis on Planktic Foraminifers and *Gephyrocapsa* Coccoliths

Carbonate samples from *Gephyrocapsa* coccolith and planktic foraminifers were analyzed at ETH Zürich on a GasBench II coupled to a Delta V isotope-ratio mass spectrometer, as described by Breitenbach and Bernasconi (2011) for small carbonate samples. The instrument was calibrated with the internal standards MS2 ($\delta^{18}O = -1.81$‰) and ETH-4 ($\delta^{18}O = -18.71$‰) to the international reference materials NBS 19 ($\delta^{18}O = -2.2$‰) and NBS 18 ($\delta^{18}O = -23.00$‰), yielding a precision of 0.07‰ for both isotopes. Values are reported in relative to the VPDB standard. Measurement replicates yielded a mean difference for oxygen and carbon isotopes of 0.04‰.

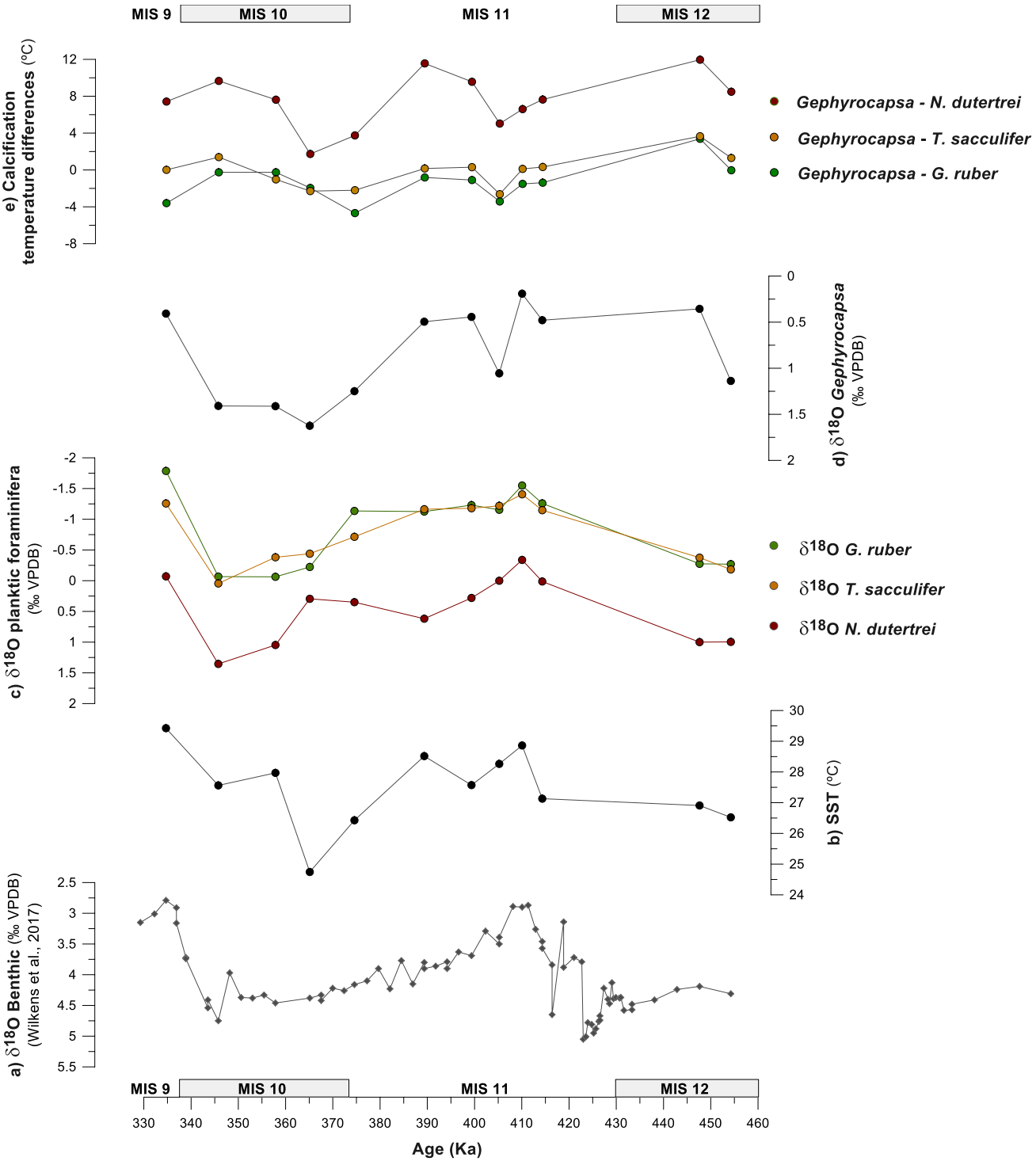

Figure 2. Changes in surface water properties across the MIS 12 to MIS 9. (a) spliced $\delta^{18}O$ benthic profile at Site 925 (‰ VPDB) by Wilkens et al. (2017); (b) $U^{k'}_{37}$ alkenone-derived SST (°C); (c) species-specific corrected $\delta^{18}O$ values of planktic foraminifera species (‰ VPDB); (d) $\delta^{18}O$ *Gephyrocapsa* (‰ VPDB); and (e) paired equilibrium calcification temperature relationships between *Gephyrocapsa* and the planktic foraminifera species (°C). Error bars of inorganic isotopic measurements are omitted for clarity and the values can be found in methods.

4.5. Calculation of ε_p and Vital Effects in Coccolith Carbon and Oxygen Isotopes

The carbon isotopic fractionation during photosynthesis (ε_p) is calculated from the carbon isotopic composition of CO_2[aq], $\delta^{13}CO_2$ and the carbon isotopic composition of the haptophyte biomass, $\delta^{13}C_{org}$, using the following equation by Jasper et al. (1994):

$$\varepsilon_p = \left[\left(\delta^{13}CO_2[aq] + 1000\right) / \left(\delta^{13}C_{org} + 1000\right) - 1\right] \times 1000 \quad (1)$$

For the estimation of $\delta^{13}C_{DIC}$, the $\delta^{13}C$ values of the planktic foraminifer *T. sacculifer* species were used. Given uncertainty about the offset between $\delta^{13}C$ *T. sacculifer* and $\delta^{13}C_{DIC}$ (e.g., Birch et al., 2013; Spero et al., 2003), we follow the practice of previous studies (Badger et al., 2019; Y. G. Zhang et al., 2020) and apply the 1‰ calcite-HCO_3^- fractionation factor, following Romanek et al. (1992), on $\delta^{13}C$ *T. sacculifer* for $\delta^{13}C_{DIC}$ estimation. Applying a different fractionation factor between foraminiferal calcite $\delta^{13}C$ and $\delta^{13}C_{DIC}$ could lead to slightly different absolute ε_p values, but would not affect the trends, neither their correlation with any variables which are discussed below. The $\delta^{13}CO_2$[aq] is calculated from $\delta^{13}C_{DIC}$, as in Benthien et al. (2002). The required temperature values are derived from the $U^{k'}_{37}$ SST at Site 925.

The $\delta^{13}C_{org}$ is obtained from the $\delta^{13}C$ of the alkenone, $\delta^{13}C_{37:2}$, following the equation that integrates the 4.2‰ fractionation factor between alkenones and cellular particulate organic carbon (Jasper et al., 1994; Popp et al., 1998):

$$\delta^{13}C_{org} = \left[\left(\delta^{13}C_{37:2} + 1000\right) \times \left(\left(4.2/1000\right) + 1\right)\right] - 1000 \quad (2)$$

The carbon isotope vital effects in *Gephyrocapsa* are calculated as the isotopic offset between the $\delta^{13}C$ *Gephyrocapsa* and $\delta^{13}C_{DIC}$ ($\Delta\delta^{13}C_{Gephyrocapsa\text{-}DIC}$), which approximates $\varepsilon_{coccolith}$. The oxygen isotope vital effect in *Gephyrocapsa* is here reported as $\Delta\delta^{18}O_{Gephyrocapsa–T.\ sacculifer}$, the isotopical offset in values between $\delta^{18}O$ *Gephyrocapsa* and the normalized to equilibrium $\delta^{18}O$ of the planktic foraminifer species *T. sacculifer*.

4.6. Coccolith Micropaleontological Analysis and Proxies

Slides for microscopic nannoplankton analysis were prepared following the random settling technique outlined by Flores & Sierro (1997). The abundance of the assemblages was estimated by counting a minimum of 400 coccoliths in a variable number of fields of view with the use of a double polarized–light *Nikon Eclipse 80i* microscope at 1000X magnification at the University of Salamanca. For coccolithophore species identification, we followed Young et al. (2003) and the guide of biodiversity the guide of biodiversity and taxonomy of coccolithophores Nannotax 3 (ina.tmsoc.org/Nannotax3). Further considerations for the recognition and classification of the species belonging to the *Gephyrocapsa* genus and grouping are found in Text S3.

The absolute coccolith abundances (coccolith g^{-1} sediment), referred as N, are calculated following Flores and Sierro (1997). N values of the total assemblage could be considered as an estimate of paleoproductivity (e.g., Baumann et al., 2005; Kinkel et al., 2000; Stolz & Baumann, 2010). From the general dependence of the r-strategists *Gephyrocapsa* species on eutrophic conditions in the upper photic zone (e.g., Barber & Hiscock, 2006; Baumann et al., 2005; Young et al., 2000), we use the N *Gephyrocapsa* spp. as a proxy to estimate the degree of nutrient-enriched surface condition in the region.

The species *F. profunda* is a common inhabitant of the deep photic zone (Kinkel et al., 2000; Okada & Honjo, 1973). Following previous authors (Beaufort et al., 1997; Molfino & McIntyre, 1990), the relationship between the percentages of *F. profunda* is used to monitor the changes in depth of the nutricline due to water column stratification.

4.7. *Gephyrocapsa* Coccolith Size, Mass, and Thickness

Slides were imaged using a *Zeiss Axiocam 506 color* camera coupled to a *Zeiss Axio Scope HAL100 POL* microscope configured with circular polarization and Zeiss Plan-APOCHROMAT 100x/1.4 Oil objective at ETH Zürich. Coccolith length, volume and mass were obtained by processing images with the C-Calcita

software (Fuertes et al., 2014). For thickness calibration, a calcite wedge manufactured at ETH Zürich was used as independent reference, giving its robust relationship between gray level and thickness (González Lemos et al., 2018). A minimum of 100 *Gephyrocapsa* coccoliths between 3 and 5 μm was analyzed. Coccolith lengths serve to derive the *Gephyrocapsa* coccolithophore cellular sizes (radius), following the dimensional relation in Noëlaerhabdaceae by Henderiks and Pagani (2007).

Following Bolton et al. (2016) and references therein, the coccolith thickness is considered as representative of the degree of calcification of coccolithophore cell. Size normalized thickness (SN thickness) was calculated to accurate the size relation of calcification for every measured coccolith by following the equation by O'Dea et al. (2014):

$$\text{SN thickness} = \left[\left(\text{ML} - \text{CL}\right) \times S\right] + \text{CT} \quad (3)$$

where ML = mean coccolith length; CL = length of each individual coccolith in sample; S = slope of the regression between length and thickness for all coccoliths in sample; and CT = original thickness of each individual coccolith in sample.

4.8. Statistical Analyses

The Pearson correlation coefficient (R) and its level of significance (p-values) are shown to assess the relationship between the proxy data produced and discussed in this study (e.g., Table 2; Figures 5, 6, 9, S7, and S8). This analysis was performed using the package GGally (https://cran.r-project.org/web/packages/GGally/index.html) in R software (R core Team, 2021). Correlations with p-values lower than or equal to the threshold of 0.05 ($p \leq 0.05$) are considered as statistically representative in this study.

Coefficients of determination (R^2) were calculated to determine how much of the variation of the predicted variable is explained by the response variable or variables (e.g., Figure 7; Tables S3–S6).

Monte Carlo error propagation was employed to constrain the uncertainty associated with the calculation of ε_p when we apply the relationships identified during the Late Quaternary (this study) on pCO_2 estimation back to the Neogene (see Section 6.4).

5. Results

5.1. Planktic $\delta^{18}O$ and Surface Ocean Temperature

Planktic foraminifer $\delta^{18}O$ and $U^{k'}_{37}$ alkenone-derived SST temperature record G-I oscillations (Figures 2b and 2c) and show significant correlations with the benthic $\delta^{18}O$ ($R = 0.92/p \leq 0.05$ and $R = -0.66/p \leq 0.05$, respectively; Figure 6). The SST records oscillate between 24 and 27°C in glacials MIS 10 and 12 and 27 and 29°C in interglacials MIS 9 and 11, with the coldest temperatures recorded at the early MIS 10 and sustained warmth during the MIS 11 interglacial (Figure 2b). The $\delta^{18}O$ trends in the three studied planktic foraminifer species closely parallel the G-I cycles observed in the benthic $\delta^{18}O$ record at Site 925 (Figures 2a and 2c). Following correction for species-specific vital effects, trends and values of *G. ruber* and *T. sacculifer* are similar, whereas *N. dutertrei* has $\delta^{18}O$ more positive than both *G. ruber* and *T. sacculifer* (by +1.3‰ and +1.24‰, respectively; Figure 2c).

The $\delta^{18}O$ *Gephyrocapsa* records a comparable G-I trend to the planktic foraminifer *G. ruber* and *T. sacculifer*, but offset to higher absolute values (Figure 2d). When specific $\delta^{18}O$ temperature calibration equations for each taxa are used to estimate calcification temperature relationships (see protocol of calculation in Text S2), assuming similar $\delta^{18}O_{sw}$ in foraminiferal and coccolithophore habitats across the photic zone, as suggested by modern monitoring (Waelbroeck et al., 2014), the calcification temperature of *Gephyrocapsa* is most similar to that of *G. ruber* and *T. sacculifer* and significantly warmer than that of *N. dutertrei* (Figure 2e).

5.2. Stratification and Export Production and *Gephyrocapsa* Morphometries

Temporal variations in the indicators of water column stratification and export production exhibit some similarities but also significant divergences. There is a large range (from 0.6‰ to 1.8‰) in the $\delta^{18}O$ gradient between *N. dutertrei* and *G. ruber* or *T. sacculifer* (Figure 3b). The lowest gradients coincide with the coldest $U^{k'}_{37}$ SST, early in MIS 10 (Figures 2b and 3b). In contrast to this large variability in the isotopic indicators of stratification, the coccolith-derived proxy of stratification, *F. profunda*, is more stable (Figure 3c). The coccolith assemblage is dominated by the *Gephyrocapsa* genus (average 70%; Figure 3d and Text S3) and the relative abundance of *F. profunda* varies only slightly between 20% and 32% (Figure 3c). These modest variations in the percentages of *F. profunda* show no consistent relationship with G-I cycles (Figure 3c), nor with the higher amplitude variations in $\Delta^{18}O_{N.\ dutertrei\text{-}G.\ ruber}$ (Figures 2b and 6).

The N of the total assemblage and *Gephyrocapsa* species is high during MIS 12 and progressively decreases by 40% within MIS 11 and MIS 10 (Figure 3f). A moderate final increase is observed at MIS 10/MIS 9 (334 ka; Figure 3f). The maintenance of high values around 1 in the CEX dissolution index (Text S4 and Figure S5) indicates a negligible dissolution effect. The alkenone C37/C38.et ratio exhibits high values from 1.75‰ to 1.95‰ at MIS 12 and generally decreases through MIS 11 and MIS 10, from 1.95‰ to 1.6‰, but exhibits more structure than the N coccolith, with local maxima at 447, 399, 374, and 357 ka (Figure 3g).

Maximum length and mass of *Gephyrocapsa* coccoliths are attained during the glacial periods (Figures 3i and 3j). A maximum mass of 8 pg characterizes the coldest part of MIS 10 glacial at 365 ka, whereas minimum mass of 6.5 pg occurs during the earlier MIS 11, at 414 ka (Figure 3j); length is significantly correlated with the benthic $\delta^{18}O$ as an indicator of G-I stages ($R = 0.56/p \leq 0.05$; Figure 6). In comparison with the measured range in modern Noëlaerhabdaceae (González Lemos et al., 2018), the SN thickness in *Gephyrocapsa* coccoliths does not vary significantly at Site 925 (Figure 3h). There is no overall correspondence between the changes in the *Gephyrocapsa* morphometrical parameters and the changes in the species composition of the *Gephyrocapsa* assemblage, because the assemblage variations are minor and not dominated by G-I cyclicity (Text S3 and Figure S5).

5.3. ε_p and Vital Effects in *Gephyrocapsa* Coccolith Carbon and Oxygen Isotopes

ε_p and $\varepsilon_{coccolith}$ are calculated using the $\delta^{13}C$ of *T. sacculifer* (Figure 4b) as an indicator of the $\delta^{13}C_{DIC}$. As this planktic foraminifer species shows a similar calcification temperature as *Gephyrocapsa* through the interval (Figure 2e), it is considered to share the most similar production depth and season as the alkenone producers. ε_p ranges from 12.1‰ to 14.3‰, and is dominantly driven by the 3‰ variation in $\delta^{13}C_{37:2}$ (Figures 4c and 4d). ε_p is higher during interglacials and lower during glacials (Figure 4d) and is significantly correlated with the benthic $\delta^{18}O$ ($R = -0.7/p \leq 0.05$; Figures 5a and 6) and the $\delta^{18}O$ of *G. ruber* ($R = -0.61/p \leq 0.05$; Figures 5b and 6).

The *Gephyrocapsa* carbon vital effects from $\varepsilon_{coccolith}$ ranges from 0.47‰, recorded at MIS 12, to 2.32‰ at MIS 10 (Figure 4f). The *Gephyrocapsa* oxygen vital effects, from $\Delta\delta^{18}O_{Gephyrocapsa\text{-}T.\ sacculifer}$, range from +0.7 to +2.2 (Figure 4g). Both the carbon and oxygen vital effect profiles increase from the lowest values at MIS 12 (447 ka) to the highest at MIS 10 (365 ka; Figures 4f and 4g).

6. Discussion

6.1. Evolution of Surface Production Environment From MIS 12 to MIS 9

Both the relative abundance of deep photic zone coccolithophore species *F. profunda* and the isotopic $\Delta\delta^{18}O$ gradient between the shallow living species *G. ruber* and *T. sacculifer* and the thermocline-dwelling *N. dutertrei* (Figures 3b and 3c) are proposed as indicators of upper water column stratification. Higher values of $\Delta\delta^{18}O_{N.\ dutertrei\text{-}G.\ ruber}$ and $\Delta\delta^{18}O_{N.\ dutertrei\text{-}T.\ sacculifer}$ are indicative of large temperature gradients that imply increased stratification (Vink et al., 2002). In oligotrophic water masses, higher percentages of *F. profunda* are linked to a deep nutricline, while low percentages characterize a shallow nutricline (e.g., Ahagon et al., 1993; Beaufort et al., 1997; Molfino & McIntyre, 1990). Compared with other oceanographic regions, the maxima $\Delta\delta^{18}O_{N.\ dutertrei\text{-}G.\ ruber}$ (1.7‰) and $\Delta\delta^{18}O_{N.\ dutertrei\text{-}T.\ sacculifer}$ (1.78‰) in this study (Figure 3b)

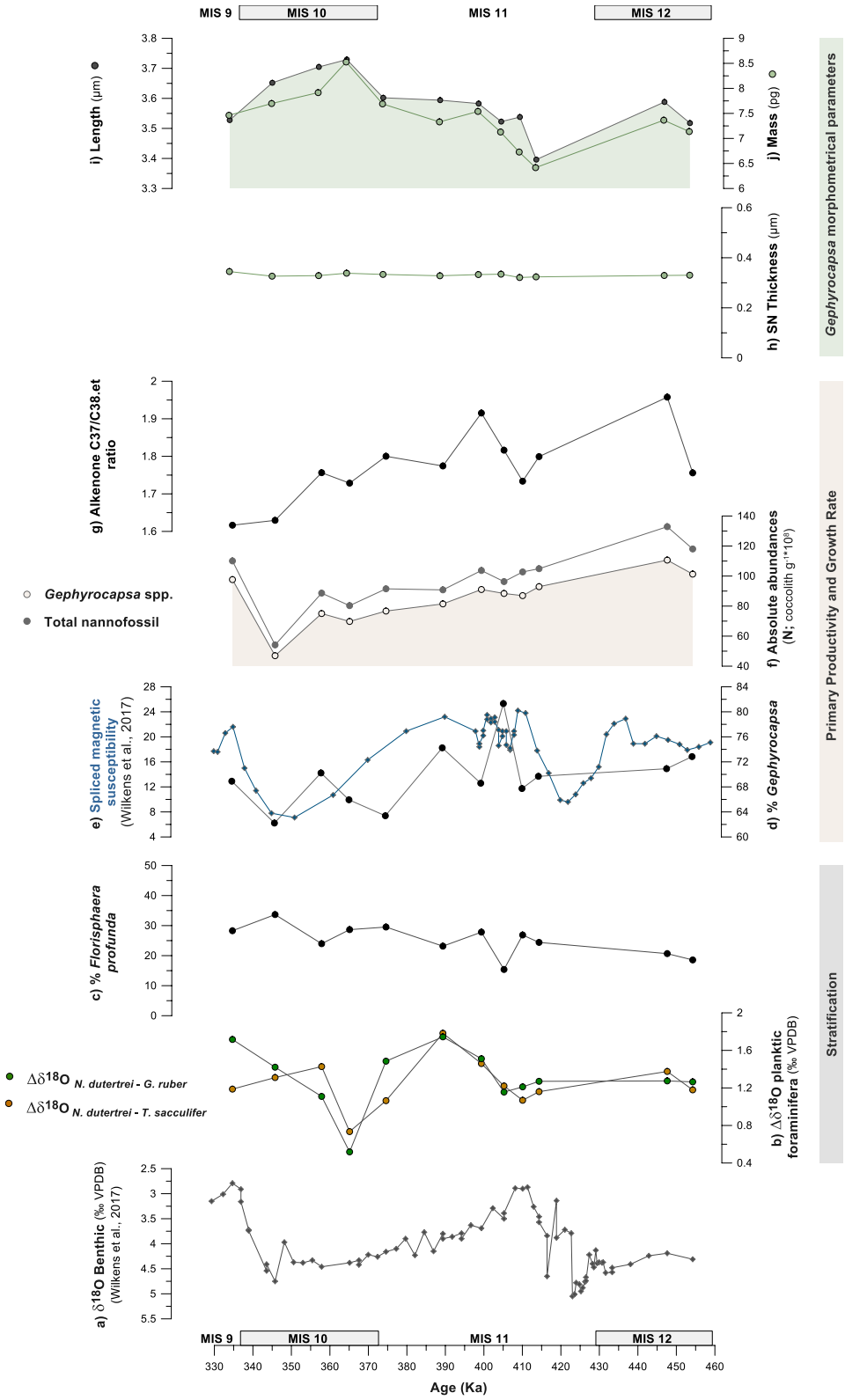
MIS 9
MIS 10
MIS 11
MIS 12
i) Length (µm)
j) Mass (pg)
h) SN Thickness (µm)
Gephyrocapsa morphometrical parameters
g) Alkenone C37/C38.et ratio
Gephyrocapsa spp.
Total nannofossil
f) Absolute abundances (N: coccolith g-1*10⁸)
e) Spliced magnetic susceptibility (Wilkens et al., 2017)
d) % Gephyrocapsa
Primary Productivity and Growth Rate
c) % Florisphaera profunda
Δδ18O N. dutertrei - G. ruber
Δδ18O N. dutertrei - T. sacculifer
b) Δδ18O planktic foraminifera (‰ VPDB)
Stratification
a) δ18O Benthic (‰ VPDB) (Wilkens et al., 2017)
Age (Ka)

Figure 3

are intermediate between those of intensely upwelled waters of the Arabian sea (1‰; Prell & Curry, 1981) and the highly stratified surface waters of the northern Panama basin (2‰; Curry et al., 1983). However, our G-I $\Delta\delta^{18}O$ estimates for the MIS 12–9 at Site 925 are similar to those observed in core tops in the region (Dekens et al., 2002) and during the last glacial cycle, from comparable $\Delta\delta^{18}O_{T.\ sacculifer–G.\ truncatulinoides}$ (Wilson et al., 2011).

The relative abundance of *F. profunda* at Site 925 is also intermediate between the low values of upwelling regions and the very high values of strongly stratified regions. Application of the global calibration of % *F. profunda* by Hernández-Almeida et al. (2019) suggests an average primary productivity of 760 mgC m^{-2} day^{-1}, also corresponding to a moderate supply of deep nutrients into the upper photic zone. These estimates are consistent with the modest growth rates modeled for Site 925 today, which are also in the intermediate range compared to other tropical settings (Krumhardt et al., 2017, Figure 1c). Although these proxies agree on the intermediate average rate of nutrient supply to the surface photic zone, $\Delta\delta^{18}O_{N.\ dutertrei-G.\ ruber}$ and $\Delta\delta^{18}O_{N.\ dutertrei-T.\ sacculifer}$ are much more variable than percentages of *F. profunda* (Figures 3b and 3c). We suggest that the minimum in $\Delta\delta^{18}O_{N.\ dutertrei-G.\ ruber}$ and $\Delta\delta^{18}O_{N.\ dutertrei-T.\ sacculifer}$ at 365 ka, coincident with the lowest SST of the record (Figures 2b and 3b) may reflect a shallowing of the depth habitat of *N. dutertrei* in response to the intense cooling, rather than a true reduction in stratification. We, therefore, more confidently interpret the *F. profunda* record and infer that the stratification and rate of mixing of the upper water column has not varied significantly at this site through MIS 12–9.

While stratification was invariant over time, the abundance of coccoliths in sediments decreases progressively from MIS 12 through MIS 9, a trend also observed as a decrease in the alkenone C37/C38.et ratio (Figures 3f and 3g). This suggests potential variation in algal growth rates and export production unrelated to changes in stratification. At the Site 925 setting, the Amazon River plume represents another source of nutrients to the upper photic zone, which are distributed in the upper 50 m of water column (e.g., Boyle et al., 1977; DeMaster et al., 1986). The magnetic susceptibility at Site 925, inferred as an indicator of Amazon-derived detrital magnetic minerals (Francois & Bacon, 1991), is significantly correlated to N *Gephyrocapsa* ($R = 0.68/p \leq 0.05$; Figure 6) and has a correspondence with the percentages of *Gephyrocapsa* (Figures 3e and 3d). This positive correlation trend is opposite to that expected if coccoliths were diluted by terrigenous input or carbonate dissolution were controlling the concentration of magnetic minerals.

The multiple linear regression of magnetic susceptibility and percentages of *F. profunda* explains 62% of the variability of N *Gephyrocapsa* (Table S3). We suggest that the decrease in *Gephyrocapsa* production was mainly triggered by a decline in delivery of nutrients from Amazon plume waters to the surface above the Site 925. The increase in percentages of *F. profunda* and decrease of N *Gephyrocapsa* from MIS 12 to MIS 9 (Figures 3c and 3f) is coherent with reduced euphotic zone fertilization, either from a decline in the surface delivery of nutrients by a limitation in the influence of Amazon plume waters above the Site 925 (Figure 3e) or a slight general deepening of the nutricline.

6.2. CO_2 and Other Environmental Influences on ε_p at Site 925

At Site 925, 48% of the variability of the measured ε_p record is explained by ln (CO_2[aq]), $R^2 = 0.48$ (Figure 7), confirming a significative influence of the changes in CO_2[aq] on ε_p across the MIS 12 to MIS 9.

The mechanistic interpretation of the relationship between ε_p and CO_2[aq] is still under debate (e.g., Badger, 2021; Stoll et al., 2019). Traditionally, the relationship has been interpreted to arise from a purely diffusive CO_2 supply across a cell into a single intracellular space in which carbon was fixed (e.g., Rau et al., 1996). Subsequently, multiple-compartment cellular models revealed that, in addition to diffusion into the cell, enhancement of the concentration of dissolved inorganic carbon in intracellular compartments, including the site of carbon fixation, could regulate the relationship between ε_p and CO_2[aq] (e.g., Cassar et al., 2006;

Figure 3. Surface production proxies: (a) spliced $\delta^{18}O$ benthic profile at Site 925 (‰ VPDB) by Wilkens et al. (2017); (b) $\Delta\delta^{18}O_{N.\ dutertrei-G.\ ruber}$ (green dots) and $\Delta\delta^{18}O_{N.\ dutertrei-T.\ sacculifer}$ (yellow dots) (‰ VPDB); (c) % *Florisphaera profunda*; (d) % *Gephyrocapsa*; (e) spliced magnetic susceptibilities at Site 925 by Wilkens et al. (2017); (f) absolute abundances, N (coccolith g^{-1}sediment), of *Gephyrocapsa* (colored section) and the total assemblage (black dots); and (g) alkenone C37/38.et ratio. *Gephyrocapsa* coccolith morphometries in samples (h) average size normalized (SN) thickness (μm). The scale is adjusted to the range of variability of modern Noëlaerhabdaceae by González Lemos et al. (2018); (i) average coccolith length (μm); and (j) average coccolith mass (pg).

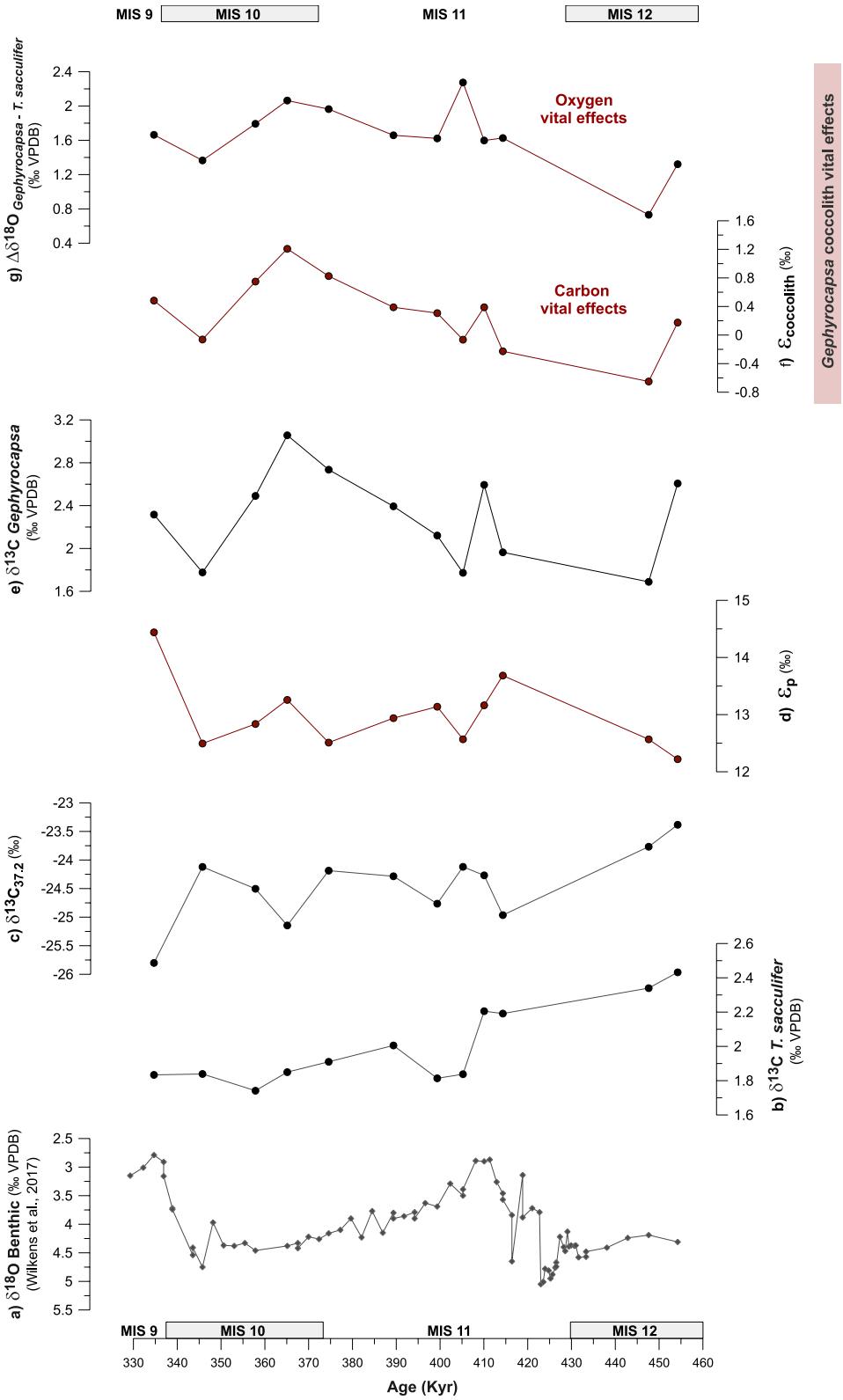
MIS 9
MIS 10
MIS 11
MIS 12
g) Δδ18O Gephyrocapsa - T. sacculifer (‰ VPDB)
Oxygen vital effects
Carbon vital effects
f) εcoccolith (‰)
Gephyrocapsa coccolith vital effects
e) δ13C Gephyrocapsa (‰ VPDB)
d) εp (‰)
c) δ13C37:2 (‰)
b) δ13C T. sacculifer (‰ VPDB)
a) δ18O Benthic (‰ VPDB) (Wilkens et al., 2017)
Age (Kyr)

Figure 4

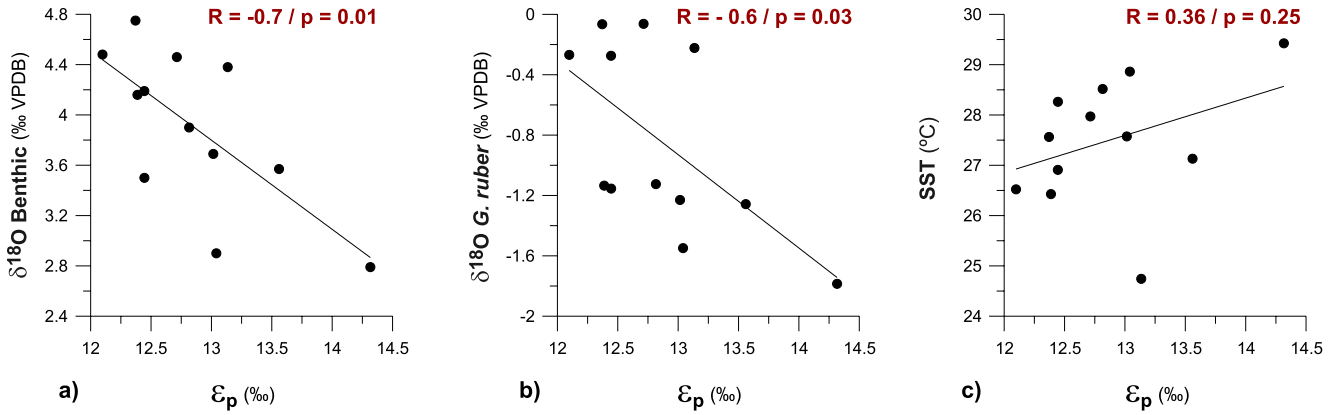

Figure 5. Relationship of ε_p with regional proxies at Site 925: (a) $\delta^{18}O$ benthic at Site 925 (Wilkens et al., 2017); (b) $\delta^{18}O$ *G. ruber*; and (c) $U^{k'}_{37}$ alkenone-derived SST (°C).

Hopkinson et al., 2011). The relationship between ε_p and CO_2[aq] found in cultured phytoplankton appears inconsistent with a purely diffusive acquisition (Stoll et al., 2019).

In this section, we review the degree to which the new data of ε_p from fossil record at Site 925 could be consistent with (a) the diffusive model (Rau et al., 1996) with varying assumptions of growth rate and the Rubisco fractionation factor (Section 6.2.1) and (b) the empirical dependence observed in laboratory cultures (Stoll et al., 2019), which is known to respond to the operation of carbon concentrating mechanisms (Section 6.2.2).

6.2.1. ε_p Compared to Predictions From Diffusive Model

According to the diffusive model of phytoplankton carbon acquisition, the increasing CO_2[aq] promotes a higher relative carbon supply to cellular demand, resulting in higher ε_p (Rau et al., 1996). Beyond this control, other environmental and physiological parameters can modify this relationship if cellular carbon requirements change: smaller cell sizes, entailing a higher surface area/volume (SA/V) ratio, or lower growth rates, would both be expected to maintain a high ratio of diffusive CO_2 supply relative to cellular carbon demand, leading as well to higher ε_p.

Using the model of Rau et al. (1996), we incorporate the measured *Gephyrocapsa* cell radius and ε_p at Site 925 together with the estimated CO_2[aq], and the recent experimental determinations of cell permeability to CO_2 by Blanco-Ameijeiras et al. (2020) to evaluate if the response of ε_p is consistent with the physical diffusive model. There are no independent determinations of absolute growth rates across the MIS 12–9 at the studied location, so we explore possible values, including (a) the application of a recently suggested regression to infer growth rates from coccolithophore cell size by Y. G. Zhang et al. (2020) (simulations A and F in Table 1 and Figure 8), (b) growth rates estimated using the PO_4 and temperature formulation by Krumhardt et al. (2017) with constant modern PO_4 (Figure 1c) and either average constant temperature (simulation E in Table 1; Figure 8b) or the $U^{k'}_{37}$ SST temperature variation at Site 925 (simulations B and G in Table 1; Figure 8), and (c) absolute growth rates used as a tuning parameter to improve agreement between the modeled and observed ε_p (simulations C and D in Table 1; Figure 8a).

When the diffusive model is applied assuming a maximum effective enzymatic Rubisco fractionation factor (ε_f) of 25‰, as traditionally simulated (Figure 8a) the modeled ε_p is significantly higher than the

Figure 4. ε_p and vital effects in *Gephyrocapsa* coccolith carbon and oxygen stable isotopes: (a) spliced $\delta^{18}O$ benthic profile at Site 925 (‰ VPDB) by Wilkens et al. (2017); (b) $\delta^{13}C_{DIC}$ calculated from $\delta^{13}C$ *T. sacculifer* (‰ VPDB); (c) $\delta^{13}C_{37:2}$ (‰ VPDB); (d) ε_p measured at Site 925 (‰ VPDB; (e) $\delta^{13}C$ *Gephyrocapsa* (‰ VPDB); (f) *Gephyrocapsa* carbon vital effects, as $\varepsilon_{coccolith}$ (‰ VPDB); and (g) *Gephyrocapsa* oxygen vital effects as $\Delta\delta^{18}O_{Gephyrocapsa\text{-}T.\ sacculifer}$ (‰ VPDB). Error bars of organic isotopic measurements are omitted for clarity and the values can be found in methods; error on ε_p is typically <0.5‰, smaller than the size of the symbol.

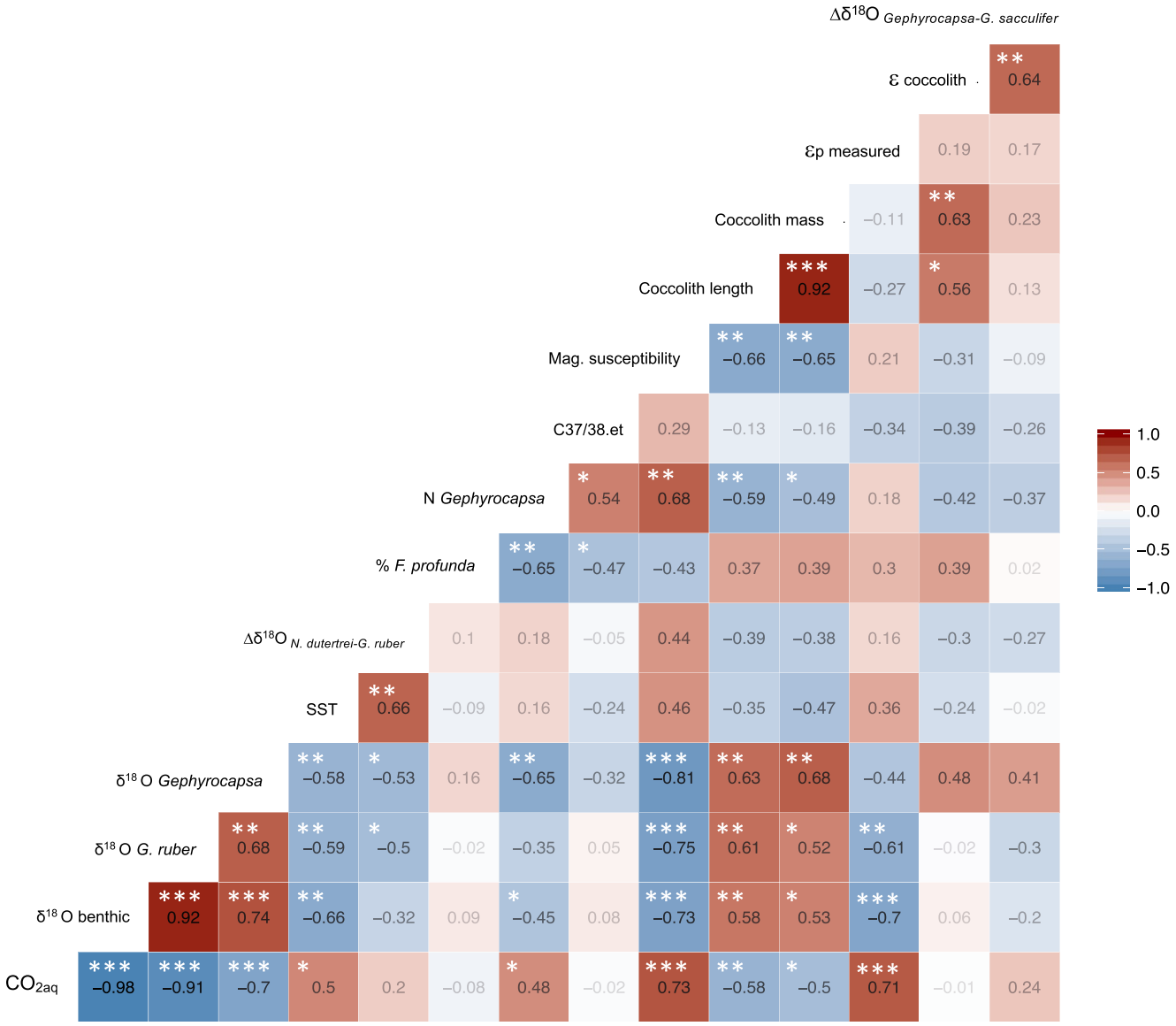

Figure 6. Pearson correlation matrix of the proxies and data in this study: CO_2[aq], $\delta^{18}O$ *G. ruber*, $\delta^{18}O$ *Gephyrocapsa*, $U^{k'}_{37}$ alkenone-derived SST, $\Delta\delta^{18}O_{N. dutertrei-G. ruber}$, *% F. profunda*, absolute values (N; coccolith g^{-1} sediment) of *Gephyrocapsa*, alkenone C37/38.et ratio, average *Gephyrocapsa* coccolith length and mass, ε_p, $\varepsilon_{coccolith}$, and $\Delta\delta^{18}O_{Gephyrocapsa-G. sacculifer}$. The spliced $\delta^{18}O$ benthic and magnetic susceptibilities at Site 925 by Wilkens et al. (2017) are also included. Symbols represent the statistical significance: ***$p \leq 0.01$; **$p \leq 0.05$ and *$p \leq 0.1$.

observations at Site 925 when growth rates are estimated (a) using the cell size regression by Y. G. Zhang et al. (2020) from the *Gephyrocapsa* cell radius at Site 925 (simulation A; Figure 8a) or (b) following Krumhardt et al. (2017) with constant modern PO_4 (Figure 1c) and variable temperature from SST at Site 925 (simulation B; Figure 8a). With ε_f of 25‰, only significantly higher growth rates lead to ε_p close to the measured values at Site 925: a constant high growth rate of 2.2 $days^{-1}$ matches the average measured ε_p, but features a much higher than observed slope of ε_p versus CO_2[aq] (simulation C; Figure 8a). However, while this growth rate matches ε_p, it is not consistent with independent estimates of the growth rate in this setting (e.g., Krumhardt et al., 2017). Only a model in which the growth rate is high but decreases significantly (26%) as CO_2[aq] decreases to glacial values, is able to reproduce the slope and absolute values of the measured ε_p at Site 925 (simulation D; Figure 8a), that is, the low sensitivity of ε_p to CO_2 would need to be caused by a compensating depression of growth rate during the low CO_2 periods. However, laboratory experiments based on half-saturation constant (K_M) for CO_2 from observations by Sett et al. (2014) suggest that growth rate is much less sensitive to CO_2 (around 6% reduction in growth rates over this range of CO_2[aq]).

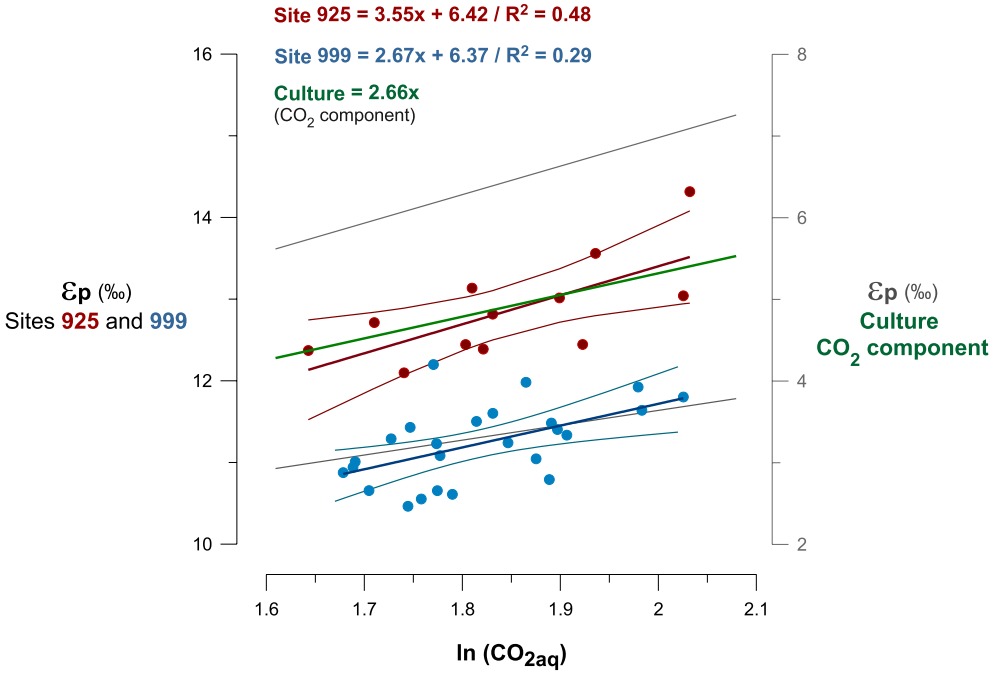

Figure 7. On the left *y*-axis: Regression of ε_p measured at Site 925 and (ln)CO_2[aq] during the MIS 12–9, in red; regression of ε_p at the nearby Site 999 and (ln)CO_2[aq] during the G-I period between MIS 8–5 (Badger et al., 2019), in blue. The best fit (lineal equation) and 95% confidence intervals are represented for both data sets. On the right *y*-axis: slope of the culture regression between the CO_2 component on ε_p and (ln)CO_2[aq] (Stoll et al., 2019), in green; the black lines represent the range of culture ε_p obtained from the upper and lower confidence interval (95% CI: 3.5 and 1.83, respectively) of the slope of the culture dependence of ε_p on CO_2 (ε_p vs. ln(CO_2[aq])).

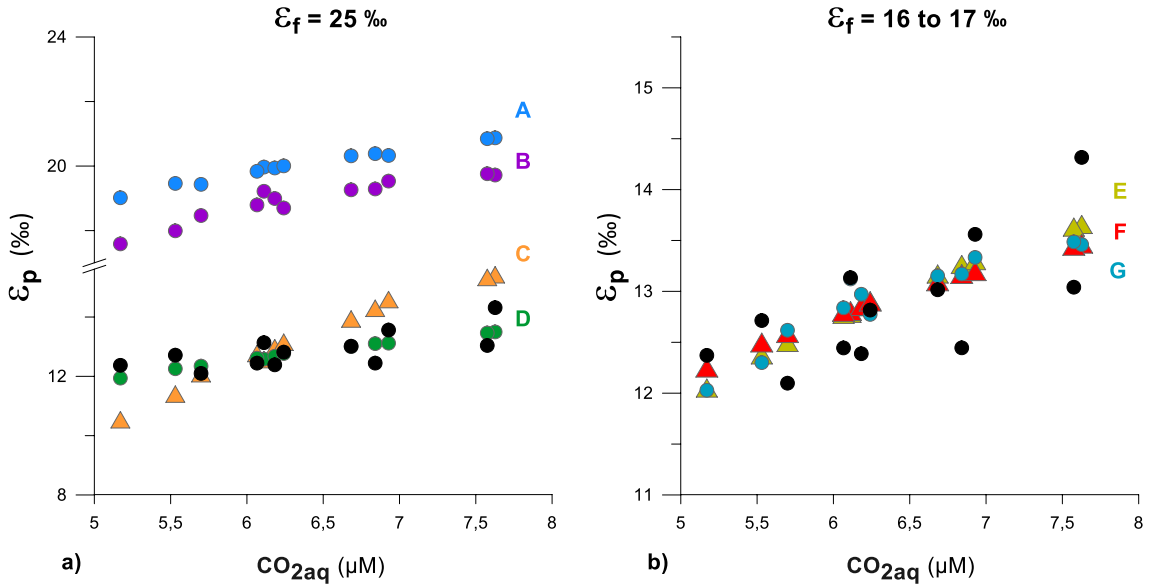

Figure 8. Regression of ε_p measured at Site 925 and CO_2[aq], in black dots, in comparison with the ε_p predicted from the diffusive model given different assumptions of (a) large Rubisco fractionation (ε_f = 25‰) or (b) lower fractionation (ε_f = 16–17‰). The different assumptions and estimations for growth rate carried out for each ε_p simulation (a) to (g) are indicated with colored symbols in the figure detailed in Table 1.

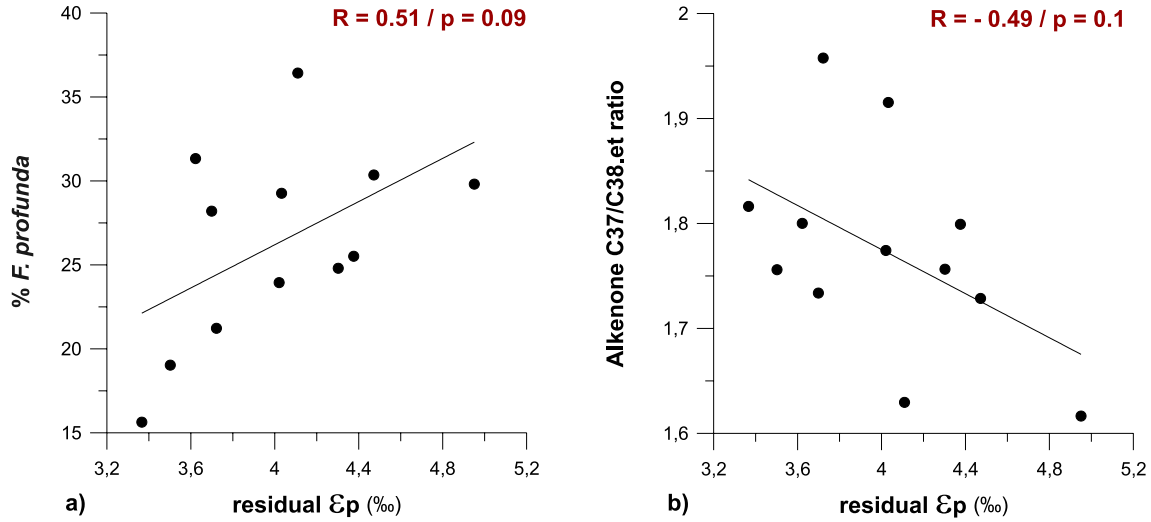

Figure 9. Correlation R of the non-CO_2 variation in ε_p (residual ε_p variation) with the surface production and growth rate proxies (a) % *Florisphaera profunda* and (b) alkenone C37/38.et ratio.

Alternatively, the low observed CO_2 sensitivity of ε_p could arise in a diffusive model due not to the influence of compensating effects of growth rate, but rather to a lower slope of the ε_p to CO_2 relationship, as would occur if ε_f were lower than 25‰ (Figure 8b). There are no ε_f data for *Gephyrocapsa* species to date, but some recent studies of Rubisco fractionation in marine eukaryotes suggest values lower than 25‰, which yield a range of 11‰–18‰ from the study of the coccolithophore species *E. huxleyi* and the diatom species *Skeletonema costatum* (Boller et al., 2011, 2015). With growth rates in the range of 0.9–1.14 day^{-1}, as obtained when estimating growth rates following both Y. G. Zhang et al. (2020) and Krumhardt et al. (2017 Table S2), the ε_p measured at Site 925 and the observed slope of ε_p versus CO_2[aq] are well matched by the ε_p diffusive simulations when ε_f values are in the range of 16‰–17‰ (simulations E–G; Figure 8b), an intermediate value between 11‰ and 18‰, which we incorporate as a sensitivity analysis. This suggests that, if the observations are to be described by diffusive model, much lower ε_f than 25‰ (Figure 8b), or a much stronger growth rate dependence on CO_2, must be used (simulations C and D; Figure 8a). However, in the Oligocene at Site 925, the measured ε_p values of 18‰–25‰ (Y. G. Zhang et al., 2013) are not compatible with an ε_f of

Table 1
Compilation of Detailed Information of ε_p Simulations From the Different Assumptions of Rubisco Fractionation (ε_f) and Growth Rate (μ) Applied to Evaluate the Adequacy of the Physical Diffusive Model (Rau et al., 1996) to Explain the Variability in ε_p Measured in Site 925.

Simulations	RMSE	εf (‰)	Estimation or assumption for μ (day^{-1})	μ variation (%)	μ average (day^{-1})
A	7.51	25	Cell size regression by Y. G. Zhang et al. (2020) from *Gephyrocapsa* cell radius at Site 925	10	0.92
B	6.38	25	Estimation by Krumhardt et al. (2017) with constant modern PO_4 and temperature variation from SST at Site 925	14	1.14
C	1.24	25	Constant high μ to minimize RMSE	0	2.2
D	0.46	25	High μ that decreases during low CO_2 (compensating depression of μ)	26	2.32
E	0.46	17	Estimation by Krumhardt et al. (2017) with constant modern PO_4 and constant temperature from average SST at Site 925	0	1.14
F	0.46	16	Average μ from cell size regression by Y. G. Zhang et al. (2020) from *Gephyrocapsa* cell radius at Site 925	0	0.92
G	0.48	17	Estimation by Krumhardt et al. (2017) with constant modern PO_4 and temperature variation from SST at Site 925	14	1.14

Note. A constant value of cell permeability (P) of 1×10^{-4} cm s^{-1} is taken from experimental determinations by Blanco-Ameijeiras et al (2020). The ε_p simulations A to G are plotted in Figure 8.
Abbreviation: RMSE, root mean square error.

Table 2
Pearson Correlation R Between the Residual ε_p and the Set of Proxies for Surface Production and Growth Rate

	$\Delta\delta^{18}O_{N.\ dutertrei\text{-}G.\ ruber}$ (‰ VPDB)	% *F. profunda*	C37/38.et	N *Gephyrocapsa*	*Gephyrocapsa* cell radius (μm)
Residual ε_p	0.0013	**0.51**	**−0.49**	−0.17	0.15

Note. The level of significance (*p*-values) is over the threshold of 0.05 in all cases, whereas bold values correspond to *p* values at least ≤0.1.

16‰, suggesting either that this is not the mechanistically correct explanation for the low G-I ε_p sensitivity or that long-term evolution of enzymes involved in carbon isotopic fractionation of alkenone producers has occurred.

In summary, the observed ε_p variations at Site 925 are not consistent with the application of the classical diffusive model, nor growth rate as a function of coccolith size, as recently proposed for other locations (Y. G. Zhang et al., 2020).

6.2.2. Comparison With Culture Observations of ε_p Dependence on CO_2

While agreeing on the influence of these same factors on ε_p, a recent culture reanalysis suggests a non-diffusive logarithmic dependence of ε_p on CO_2 (see Stoll et al., 2019).

In the regression between the ε_p record at Site 925 and ln (CO_2[aq]) across the MIS 12 to MIS 9, we obtained a slope value of 3.55 (Figure 7). Our estimated slope is on the upper end of that inferred from laboratory cultures (95% confidence interval; 1.83 to 3.5) by Stoll et al. (2019), suggesting (a) a similar sensitivity of ε_p to CO_2[aq] on ε_p at Site 925 as observed in cultures and (b) supporting the further application of the ε_p multiple regression statistical model by Stoll et al. (2019) to provide a suitable quantification of the effect of other non-CO_2 parameters on ε_p at Site 925.

The slope between ε_p and ln (CO_2[aq]) of 2.67 at the Site 999 through the MIS 8 to MIS 5 G-I cycles studied by Badger et al. (2019, Figure 7), is within the 95% confidence interval by Stoll et al. (2019). This record comes from the western Caribbean Sea, so both locations of Sites 925 and 999 are assumed to share comparable air-sea equilibrium conditions and absence of remarkable upwelling activity across the Pleistocene (see Badger et al., 2019 and references therein). The comparison suggests a similar phytoplankton sensitivity to changing G-I pCO_2 across the Pleistocene, from the MIS 12 to MIS 9 in our record and through the MIS 8–5. ε_p over the interval between 20 and 430 ka (from MIS 12 to the last glacial maximum) at ODP 925 was reported by Y. G. Zhang et al. (2013), and although the absence of reported benthic $\delta^{18}O$ for the sampled intervals leads to greater uncertainty in the estimation of the CO_2[aq], these data also show a similar sensitivity of ε_p to CO_2[aq] (see Text S1 and Figure S3).

6.2.3. Evaluating the Non-CO_2 Influences on ε_p and Potential Proxies for Them

Because the slope of ε_p relative to CO_2[aq] at 925 is similar to that of cultures by Stoll et al. (2019), but the cultures are defined by a larger data set and, therefore, a narrower confidence interval, we employ the slope from cultures to evaluate the non-CO_2 influences on ε_p in our record at Site 925. Unlike the diffusive model, the regression model is empirical and not dependent on quantifying the ε_f, nor *a priori* assumptions about the significance of diffusive versus active carbon supply (CCMs) to photosynthesis. We have chosen the culture regression with a limited range of $\delta^{13}C_{DIC}$, consistent with expectations for the Late Quaternary, and the model which provided the highest experimental R^2 value (see Stoll et al., 2019). In this model, ε_p is a combination of the influence of CO_2[aq], growth rate (μ), cell radius and light as:

$$\varepsilon_p \sim a \times \ln CO_2 + b \times \ln\ \text{light} + c \times \mu + d \times \text{radius} \quad (4)$$

As approximately 50% of variance on ε_p at Site 925 is attributed to CO_2 (Figure 7), the remaining 50% may arise due to temporal variation in cell radius, light, or growth rate. Of these parameters, we have direct estimates only for *Gephyrocapsa* cell radius from coccolith length (Figure 3i), in which increasing radius toward MIS 10, from minima values at MIS 11, is similar to that shown for the same time interval in the equatorial Pacific by Beaufort et al. (2020). The *Gephyrocapsa* cell radius values at Site 925 from coccolith length show, however, a non-significant correlation with ε_p ($R = -0.27/p \geq 0.05$; Figure 6). This fact suggests that such

changes across the MIS 12 to MIS 9 did not exert significant modulation on ε_p. In effect, the calculation of the effect of *Gephyrocapsa* cell radius on ε_p at 925 by applying the slope of size effect from the culture observations by Stoll et al. (2019) suggests that such a small size variation would affect ε_p by less than 0.14‰, a difference that we consider negligible.

Using the estimated CO_2[aq] and the values of *Gephyrocapsa* cell radius for each sample, we predict the CO_2 and cell size components of ε_p at Site 925 by applying the ε_p multiple regression model with the coefficient values and a fixed intercept from culture ($a = 2.66$, $d = -1.28$ and intercept = 6.30; see Stoll et al., 2019). The residual difference of the measured ε_p at Site 925 minus this calculated variation in ε_p (residual ε_p variation) reflects the summed effects of light and growth rate contributing to ε_p at Site 925.

Analysis of ε_p in core tops suggests that some micropaleontological proxies have a strong correlation with spatial variations in the light or growth rate effects on ε_p in the modern ocean (Hernández-Almeida et al., 2020). For our sample set, the residual ε_p variation has not statistically significant correlation with some proxies for surface production and growth rate ($p > 0.05$; Table 2). However, some relationships are observed. The comparison with percentages of *F. profunda* results in some correlation of $R = 0.51$ ($p > 0.05$; Table 2 and Figure 9a). In addition, the alkenone C37/C38.et ratio has an inverse relationship with the residual non-CO_2 variation in ε_p, $R = -0.49$ ($p > 0.05$; Table 2 and Figure 9b). On the other hand, the residual non-CO_2 variation in ε_p is not significantly correlated with the $\Delta\delta^{18}O_{\textit{N. dutertrei-G. ruber}}$, $R = 0.001$ ($p > 0.05$; Table 2), nor with N *Gephyrocapsa*, $R = -0.17$ ($p > 0.05$; Table 2). It is important to note that N *Gephyrocapsa* may not accurately reflect the production of *Gephyrocapsa* if the growth rate may be decoupled from the standing stock and total biogenic export.

The positive relationship between the percentages of *F. profunda* and the non-CO_2 ε_p is consistent with lower growth rates (or higher light) during periods of increased % *F. profunda*. The inverse relationship between the alkenone C37/38.et ratio is consistent with higher growth rates (or lower light) during periods of higher C37/38.et. This is in agreement with Herbert et al. (2018), who proposed a correlation of the C37 to C38 organic compounds with algal growth rates. The combination of percentages of *F. profunda* and the values of C37/38.et does not explain additional variation nor increased significance, with $R^2 = 0.34$ (Table S4), suggesting that both are indicating similar aspects of *Gephyrocapsa* growth and that other factors influencing ε_p are not yet resolved by the existing proxy suite.

We next evaluate if we can establish a quantitative estimation of the growth rate ε_p variation from the use of micropaleontological proxies in this study. On a regional scale, the percentages of *F. profunda* has been established as a proxy for surface ocean [PO_4^{3-}] from the study of surface sediment samples by Hernández-Almeida et al. (2020). When the [PO_4^{3-}] obtained applying that same regression (0.28–0.38 μM; Figure S6c) is incorporated into the growth rate parametrization by Krumhardt et al. (2017), we estimate growth rates ranging from 1.4 to 1.6 day^{-1} (Figure S6d). According to the steep dependence of ε_p on growth rate in cultures, this 0.2 day^{-1} variation in growth rate would be expected to lead to 1.4‰ variations in ε_p, similar to 1.5‰ found in this study. However, comparing the growth rates values estimated from this calculation with the measured ε_p at Site 925 is more difficult because the light level during *Gephyrocapsa* growth is not independently constrained. If *Gephyrocapsa* was produced at 50 m depth under modern conditions, yearly average light would be 113 μE m^{-2} s^{-1}, whereas if it was deeper between 60 and 70 m, the value would be lower, between 62 and 84 μE m^{-2} s^{-} (further details on this calculation and resulting values are included in Text S6 and Table S7). Nevertheless, we note that the parametrized growth rates using the estimation of [PO_4^{3-}] from percentages of *F. profunda* are higher than the modern modeled values (1–1.25 day^{-1}; Krumhardt et al., 2017, Figure 1c), suggesting that the approach using *F. profunda* may overestimate [PO_4^{3-}] at this location during MIS 12–9 compared to the more open ocean settings from which the calibration was developed.

We finally explore if there is a relationship between the variability in *Gephyrocapsa* cell radius and growth rate during the MIS 12 to MIS 9, since larger cell sizes have higher nutrient requirements to attain a given growth rate. For this, we used the culture regression from different studies of the K_M for growth limited by the concentration of NO_3 as a function of the cell radius (Cermeño et al., 2011; Eppley et al., 1969; Perrin et al., 2016; Riegman et al., 2000). The difference between the derived K_M NO_3 values from the smallest and largest size values at Site 925 is of about 0.075 μM, a maximum variability of too small magnitude to

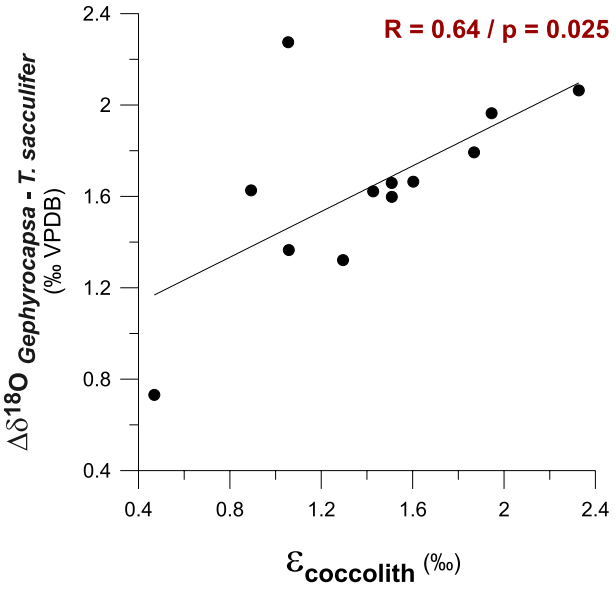

Figure 10. Correlation R between carbon and oxygen vital effects in *Gephyrocapsa* coccolith calcite at Site 925, respectively, represented from $\varepsilon_{coccolith}$ and $\Delta\delta^{18}O_{Gephyrocapsa\text{-}T.\ sacculifer}$.

exert a significant modulation on the *Gephyrocapsa* growth rates across the interval. We neither find a significant correlation between the *Gephyrocapsa* size trends and the residual ε_p ($R = 0.15/p > 0.05$; Table 2). This suggests that *Gephyrocapsa* cell sizes is a poor predictor of the growth rate or light variation effects on ε_p through MIS 12 to MIS 9 at Site 925.

6.3. Carbon and Oxygen Vital Effects in *Gephyrocapsa* Coccolith Calcite

Until this study, well-separated near monogeneric coccolith records examined for *Gephyrocapsa* vital effects spanning G-I cycles had been only made by Jin et al. (2018). Some previous studies have used bulk carbonate samples from the Caribbean Sea without quantification of the relative abundance of different coccolith species (e.g., Hermoso, 2016) or, alternatively, fine fractions in which analyses of the species abundances revealed systematic variation in assemblage (i.e., *F. profunda*) over G-I cycles (e.g., Mejía et al., 2014; Stoll et al., 2019). Because different coccolith sizes and genera are known to have contrasting isotopic fractionation (e.g., Candelier et al., 2013; Dudley et al., 1986; Hermoso et al., 2014; Rickaby et al., 2010; Ziveri et al., 2003), in mixtures with varying contribution of different groups, it is not possible to distinguish the effect of species-specific offsets from changes in stable isotope vital effects due to environmental and biological factors. Here, the specimens of the genus *Gephyrocapsa* represent the 84%–91% of the 3–5-μm microfiltered coccolith size fraction. We therefore examine to what extent the isotopic composition differs from that of coeval planktic foraminifera, to evaluate possible environmental influences on the vital effects in carbon and oxygen isotopes.

The carbon isotope vital effect from $\varepsilon_{coccolith}$ is significantly correlated with the vital effect in oxygen isotopes in coccoliths from $\Delta\delta^{18}O_{Gephyrocapsa\text{-}T.\ sacculifer}$ ($R = 0.64/p \leq 0.05$; Figures 6 and 10). There is no correlation between the vital effects in *Gephyrocapsa* and the changes in the assemblage structure in our record (Figures 4f, 4g, and S5), so we suggest that the vital effect is not controlled by the changes in the species composition of the *Gephyrocapsa* assemblage through time. In contrast we suggest a variable physiological effect in Noëlaerhabdaceae on the magnitude of stable isotope fractionation in coccolith calcite, in agreement with previous studies (e.g., Bolton & Stoll, 2013; Hermoso et al., 2015).

6.3.1. Carbon Isotope Vital Effects

Cell modeling suggests that the $\varepsilon_{coccolith}$ may increase with higher photosynthetic rates and low CO_2[aq] (Bolton & Stoll, 2013; Holtz et al., 2017; McClelland et al., 2017). The reason is that photosynthesis fractionates against the heavy isotope, so the intracellular DIC pool is more positive when there is a higher photosynthetic rate, resulting in higher $\delta^{13}C$ of the carbon available for calcification. In this sense, faster growth rates may result in a higher $\varepsilon_{coccolith}$ (Holtz et al., 2017). When the CO_2[aq] is low and the diffusive CO_2 flux is low, this isotopically heavy carbon may remain a more significant fraction of the intracellular DIC pool; conversely, at high CO_2[aq], a significant CO_2 influx may dilute the intracellular carbon pool. These processes driving an internal isotopically heavy signature could be incorporated into coccolith vesicle and recorded by $\varepsilon_{coccolith}$. In addition, the inorganic/organic carbon (PIC/POC) ratio in some circumstances is modeled to affect as well the $\varepsilon_{coccolith}$: a higher $\varepsilon_{coccolith}$ is expected to result from low PIC/POC (McClelland et al., 2017).

However, the variations in $\varepsilon_{coccolith}$ in our new record are not readily explained by the processes simulated in models. For example, although $\varepsilon_{coccolith}$ varies by over 1‰ in our record (Figure 4f), we observe a non-significant correlation with CO_2[aq], $R = -0.01$ ($p > 0.05$; Figures 6 and S8a). This contrasts with the previous results on non-monogeneric coccolith fractions from the last 200 kyr at Site 925, which evidenced correlation of higher $\varepsilon_{coccolith}$ with lower CO_2[aq] (Stoll et al., 2019). We suggest that the resulting $\varepsilon_{coccolith}$ record for the samples younger than 200 ka not dominated by species of the genus *Gephyrocapsa* may reflect the impact of major changes in the coccolithophore assemblages rather than CO_2 on isotopic fractionation in a given

species. Thus, our new results suggest that non-CO_2 aspects of the surface production conditions may exert dominant effect on the *Gephyrocapsa* $\varepsilon_{coccolith}$ across the MIS 12 to MIS 9. For example, while low CO_2[aq] is expected to increase $\varepsilon_{coccolith}$, such a signal could be obscured if there were a compensating process working to decrease $\varepsilon_{coccolith}$ at low CO_2 effect, such as (a) a reduced growth rate or (b) an increase in PIC/POC. Regarding the latter mechanism, since coccolith SN thickness has a negligible variation among our samples (Figure 3h), we have no evidence for significant changes in the degree of cellular calcification (PIC/cell surface area) or PIC/POC. There are positive correlations between $\varepsilon_{coccolith}$ and *Gephyrocapsa* coccolith length R = 0.56 (Figure 6) and mass R = 0.63 (Figure 6). If the ratio of cellular carbon supply to demand correlated with coccolith size and SA/V ratio, then larger sizes might be expected to increase the $\varepsilon_{coccolith}$ (McClelland et al., 2017), as we observe (Figures 3i and 4f). However, while this process is working in the expected direction, its magnitude may not be sufficient: in cellular process models, a 1‰ shift in $\varepsilon_{coccolith}$ would require a 60% increase in carbon utilization (McClelland et al., 2017). The maximum range in *Gephyrocapsa* coccolith length (size) is <10% (Figure 3i).

$\varepsilon_{coccolith}$ shows a non-significant correlation with the surface production proxies of % *F. profunda* (R = 0.39/p > 0.05; Figure 6) and N *Gephyrocapsa* (R = −0.42/p > 0.05; Figure 6), and the growth rate proxy C37/C38.et (R = −0.39/p > 0.05; Figure 6) and the sign of this relationship is opposite to that predicted by cellular process models. It is important to note that the percentages of *F. profunda* and C37/C38.et have the expected correlation for growth rate effect on ε_p (Section 6.2.3). These results evidence that the variations in growth rate or production indicated by these proxies do not influence $\varepsilon_{coccolith}$ in the manner predicted by cellular process models, as neither have a significant influence individually on $\varepsilon_{coccolith}$. However, it is possible that these growth rate and production proxies contain complementary information that helps to explain a higher proportion of the $\varepsilon_{coccolith}$ variance when they are combined. Thus, when we combine in a multiple linear regression model the *Gephyrocapsa* coccolith mass and the C37/C38.et to predict $\varepsilon_{coccolith}$, the explained variance is higher, $R^2 = 0.49$ (Table S5), and even higher with the addition of CO_2[aq] to the previous variables, improving the performance of the multiple linear regression model ($R^2 = 0.59$; Table S6).

6.3.2. Oxygen Isotope Vital Effects

The $\Delta\delta^{18}O_{Gephyrocapsa\text{-}T\ sacculifer}$ values (Figure 4g) are consistent with previous studies, showing *Gephyrocapsa* to have higher $\delta^{18}O$ than equilibrium calcite (Dudley et al., 1986; Hermoso et al., 2015; Ziveri et al., 2003). The temporal variation in $\Delta\delta^{18}O_{Gephyrocapsa\text{-}T.\ sacculifer}$ is >1‰, suggesting that recent assumptions of a constant $\Delta\delta^{18}O_{Gephyrocapsa\text{-}T.\ sacculifer}$ for paleoceanographic studies (e.g., Hermoso et al., 2020; Tremblin et al., 2016 and references therein) may require reevaluation. More specifically, our results from time series are in agreement with core-top calibration by Hermoso et al. (2015), in which Noëlaerhabdaceae $\delta^{18}O$ may be controlled by multiple factors in addition to temperature.

Positive correlation between oxygen and carbon isotope vital effects among coeval coccolith populations of different species from sediments (Bolton & Stoll, 2013), core top sediments (Hermoso et al., 2015), or among species in culture (Ziveri et al., 2003) has been widely described but seldom documented in time series (e.g., Hermoso et al., 2020; Jin et al., 2018; Liu et al., 2002). The main physiological mechanisms alluded as triggering Noëlaerhabdaceae $\delta^{18}O$ enrichment from equilibrium has been (a) intracellular pH reduction in the coccolith vesicle (Hermoso et al., 2015; Ziveri et al., 2003, 2012) and (b) the effect of fast growth rates on the DIC pool signature (e.g., Hermoso et al., 2014). However, coupled models of carbon and oxygen isotope vital effects are not yet published. This data set could be an important model target.

As observed for $\varepsilon_{coccolith}$, CO_2[aq] is not a main control of the oxygen vital effects from a low and non-significant correlation R = 0.23 (p > 0.05; Figures 6 and S8b). As suggested by Jin et al. (2018) for the Western Equatorial Pacific, it is possible that the narrow range of CO_2[aq] variability across the studied interval (~5–8 μM; Figure S2) was not significant enough to affect the $\delta^{18}O$ *Gephyrocapsa*. Whereas some albeit limited correlations between productivity proxies and carbon isotope vital effects were found, there are no significant correlations between the oxygen isotope vital effects and the surface production and growth rate proxies in our study as % *F. profunda* (R = 0.02/p > 0.05; Figure 6), N *Gephyrocapsa* (R = −0.37/p > 0.05; Figure 6), and C37/C38.et (R = −0.28/p > 0.05; Figure 6).

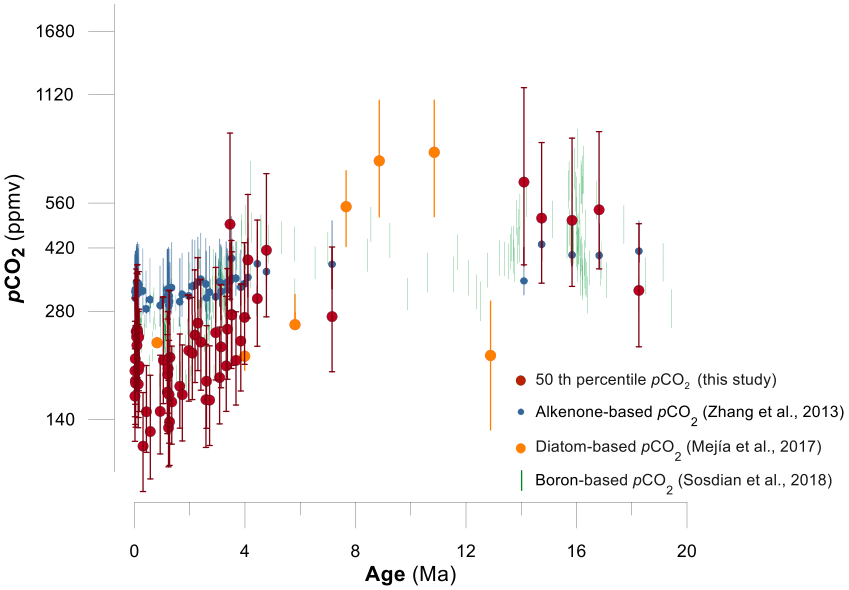

Figure 11. pCO_2 estimated at Site 925 from the MIS 12 to MIS 9 (Late Quaternary) data set and Monte Carlo error propagation through the Neogene: red dots are the 50th percentile resulting from pCO_2 estimates and the red bars represent the Monte Carlo error propagation between the 16th and 84th percentiles. Previously published pCO_2 records are showed for comparison as colored symbols: blue = alkenone ε_p-based pCO_2 by Y. G. Zhang et al. (2013); yellow = diatom ε_p-based pCO_2 by Mejía et al. (2017); and green = boron-based pCO_2 updated calculations reported in Sosdian et al. (2018).

6.4. Implications for Neogene pCO_2 Estimation at Site 925

At Site 925, previous studies reported alkenone ε_p through the Neogene (e.g., Pagani et al., 2011; Y. G. Zhang et al., 2013). Our results spanning MIS 12 to MIS 9 at Site 925 confirm that ε_p at this location is significantly influenced by the changes in CO_2[aq], with a sensitivity similar to that inferred through culture regressions (Stoll et al., 2019). So, we aim to evaluate the implications of the relationships identified in this fossil proxy data set during the Late Quaternary for longer term Neogene pCO_2 reconstruction.

From this relationship, we calculate the range of CO_2[aq] consistent with Neogene ε_p to compare it with previous calculations, which employed the classical diffusive model to derive the CO_2[aq]. The Neogene data set does not include potential proxies for growth rate, such as % *F. profunda* nor alkenone C37/38.et ratio, nor continuous data on the size of coccoliths in the time slices for which ε_p was analyzed. Consequently, as in previous interpretations, this exercise assumes that the magnitude of growth rate and other non-CO_2 contributions to ε_p has remained invariable through the Neogene. Regardless of whether this assumption is correct, we can evaluate the effect of applying an ε_p to CO_2 calibration similar to the sensitivity observed during the MIS 12 to MIS 9 glacial, versus applying a calibration based on using the classic diffusive model.

As there are no size, growth rate, or light data, we simplify the culture-based statistical calibration equation by Stoll et al. (2019) to:

$$\varepsilon_p = m\left(\ln CO_2\left[aq\right]\right) + I \tag{5}$$

where m is the slope (2.66 ± 0.42 1 s.d.) derived from cultures (see Stoll et al., 2019) and I is the intercept which encompasses, in aggregate, all other controls on ε_p. We estimate I from the Late Quaternary data set in this study (7.88 ± 0.4 1 s.d.). Given uncertainty about the offset between foraminiferal calcite $\delta^{13}C$ and $\delta^{13}C_{DIC}$, a slightly different I value from the Late Quaternary anchoring would be obtained from an initial selection of a different fractionation factor; however, it is important to note that this it would not change the slope of the ε_p versus CO_2[aq] relationship during the Late Quaternary, nor the pCO_2 estimate from Neogene recalculated ε_p data. We implement this equation in a Monte Carlo error propagation, which also incorporates the following normally distributed uncertainty in terms employed for ε_p calculation and for

pCO_2 calculation using Henry's Law: salinity: (s.d. = 1 psu), temperature (s.d. = 2°), $\delta^{13}C_{37:2}$ (as reported or s.d. = 0.2‰), and $\delta^{13}C$ foraminifera (s.d. = 0.1‰).

When calculated with the sensitivity observed in cultures (Stoll et al., 2019) and over the MIS 12–9, Neogene pCO_2 declined over the last 5 Myr at an average rate of 26 ppm per Myr (50th percentile values; Figure 11). The values for the four points in the mid-Miocene (~14–17 Ma) range from 500 to 640 ppmv, with one significantly higher pCO_2 estimate of 836 ppm in the earliest Miocene (Figure 11). Further comparison to other pCO_2 proxy records can be found in the recent review by Rae et al. (2021).

The temperature history at this site suggests minimal cooling over the Neogene (e.g., Y. G. Zhang et al., 2013), in contrast to mid and high latitude sites (e.g., Herbert et al., 2016). If the temperature change over the Neogene at Site 925 is underestimated and Miocene temperatures were significantly warmer than estimated (Y. G. Zhang et al., 2013), then the CO_2 solubility would be underestimated and the absolute pCO_2 likewise underestimated. Furthermore, if higher temperatures would suggest a higher growth rate, the use of constant growth rate over time might underestimate the amplitude of pCO_2 change.

From the relationships observed in our fossil data set, we suggest that (a) the diffusive model and conventional parameters ($\varepsilon_f = 25‰$) provide a poor fit to the ε_p during the Late Quaternary CO_2 variations (Section 6.2.1) and consequently (b) the previously published Neogene pCO_2 estimates calculated with these parameters reveal more stable pCO_2 estimates, particularly over the last 5 Myr (e.g., Y. G. Zhang et al., 2013). Alternatively, if the diffusive model was configured to fit Late Quaternary observations, for example, with $\varepsilon_f = 16‰$, it would imply mean b values of 19 (±3.15 s.d.) for the Late Quaternary. Application of this parameter set would yield an average decline of 37 ppm per Myr in the last 5 Myr, and mid-Miocene pCO_2 estimates around 500 ppmv. Therefore, when the parameters for calculation of Neogene pCO_2 are adjusted to fit the observed Late Quaternary G-I ε_p sensitivity at Site 925 (Figure 11), similar pCO_2 estimates are obtained regardless of whether a diffusive-based or empirical culture-based calibration approach is employed. However, because $\varepsilon_f = 16‰$ is not consistent with Paleogene ε_p, we suggest that tuning ε_f is not the optimal approach for past pCO_2 reconstruction.

7. Conclusions

The integration of organic geochemical (SST from alkenone $U^{k'}_{37}$ and the C37/C38.et ratio), micropaleontological (amount of *Gephyrocapsa* per gram and % *F. profunda*), geochemical (stable isotope $\delta^{18}O$ and $\delta^{13}C$ in planktic foraminifera species), and *Gephyrocapsa* coccolith morphometrical (average length, mass, and SN thickness) data analyzed on the same samples allowed us to explore different options to differentiate and evaluate the load of CO_2 and non-CO_2 effects on ε_p.

We found that phytoplankton ε_p sensitivity on CO_2[aq] across the G-I cycles from MIS 12 to MIS 9 (454–334 ka) at the Western Tropical Atlantic is consistent with the observation in cultures (Stoll et al., 2019) and in the western Caribbean (Badger et al., 2019). This sensitivity is much lower than that predicted by the classically applied model of diffusive phytoplankton CO_2 acquisition. The diffusive model, with or without the effect of cell size or growth rate variations estimated by size, provides a poor fit to our ε_p data. This result suggests that if ε_p is to be applied for CO_2 estimation, at least in tropical oligotrophic settings, the classic diffusive model may significantly underestimate both the variability and absolute pCO_2 concentrations. For such sites, either empirical relationships anchored to known Late Quaternary ice core pCO_2 concentrations, or the empirical multiple regression model from cultures by Stoll et al. (2019), may provide more robust estimates, at least for the late Neogene. We provide an example of the recalculated pCO_2 since the Miocene from published ε_p at Site 925, illustrating solely the effect of the ε_p sensitivity to CO_2 on the calculation.

Our analysis suggests that, at least at some sites, further improvements to pCO_2 estimation may be possible using additional indicators of non-CO_2 effects on ε_p. We found that % *F. profunda* and the alkenone C37/38.et ratio were able to explain part of the non-CO_2 variability. At Site 925, this may reflect a marked fertilization response of the coccolithophore species of the *Gephyrocapsa* genus to the surface nutrient input triggered by Amazon-affected waters that may have an effect on the changes in growth rate and light levels through the interval.

This data set further provides clear evidence of coupled models of carbon and oxygen isotope vital effects in *Gephyrocapsa* coccolith calcite trough the MIS 12 to MIS 9, but further evaluation with cellular process models for vital effects is needed for a quantitative understanding of the drivers of these effects.

Data Availability Statement

All original data produced for this work is available at the public repository Mendeley as: González-Lanchas, Alba; Stoll, Heather; Hernández-Almeida, Iván; Flores, José-Abel; Sierro, Francisco J.; Guitián, José (2020), "Carbon isotopic fractionation of alkenones and *Gephyrocapsa* coccoliths over the Late Quaternary (Marine Isotope Stages 12 to 9) glacial-interglacial cycles at the western tropical Atlantic," Mendeley Data (https://data.mendeley.com/datasets/zhmwhjjs63).

Acknowledgments
This study was supported by the predoctoral FPU contract FPU17/03349 and the program EST18/00842 for a research stay at Climate Geology Group (ETH Zürich), both awarded to A. González-Lanchas by the Spanish Ministry of Science, Innovation and Universities. Financing infrastructure was provided by the programs RTI2018-099489-B-100 of the Spanish Ministry of Science, Innovation and Universities granted to GGO (Grupo de Geociencias Oceánicas de la Universidad de Salamanca) and by the Swiss National Science Foundation award 200021_182070 granted to H.M. Stoll. Authors appreciate the suggestions and comments of the four anonymous reviewers, which benefited the manuscript. The authors also thank Madalina Jaggi for her assistance in the laboratory and Thomas Tanner for the guidelines on the procedure for the extraction and treatment of organic compounds.

References

Ahagon, N., Tanaka, Y., & Ujiie, H. (1993). Florisphaera profunda, a possible nannoplankton indicator of late Quaternary changes in sea-water turbidity at the northwestern margin of the Pacific. *Marine Micropaleontology*, *22*, 255–273. https://doi.org/10.1016/0377-8398(93)90047-2

Aurahs, R., Treis, Y., Darling, K., & Kucera, M. (2011). A revised taxonomic and phylogenetic concept for the planktonic foraminifer species Globigerinoides ruber based on molecular and morphometric evidence. *Marine Micropaleontology*, *79*, 1–14. https://doi.org/10.1016/j.marmicro.2010.12.001

Bach, L. T., Mackinder, L. C., Schulz, K. G., Wheeler, G., Schroeder, D. C., Brownlee, C., & Riebesell, U. (2013). Dissecting the impact of CO_2 and pH on the mechanisms of photosynthesis and calcification in the coccolithophore Emiliania huxleyi. *New Phytologist*, *199*, 121–134. https://doi.org/10.1111/nph.12225

Bach, L. T., Riebesell, U., & Schulz, K. G. (2011). Distinguishing between the effects of ocean acidification and ocean carbonation in the coccolithophore Emiliania huxleyi. *Limnology & Oceanography*, *56*, 2040–2050. https://doi.org/10.4319/lo.2011.56.6.2040

Badger, M. P. (2021). Alkenone isotopes show evidence of active carbon concentrating mechanisms in coccolithophores as aqueous carbon dioxide concentrations fall below 7 μmol L^{-1}. *Biogeosciences*, *18*(3), 1149–1160. https://doi.org/10.5194/bg-18-1149-2021

Badger, M. P., Chalk, T. B., Foster, G. L., Bown, P. R., Gibbs, S. J., Sexton, P. F., et al. (2019). Insensitivity of alkenone carbon isotopes to atmospheric CO_2 at low to moderate CO_2 levels. *Climate of the Past*, *15*, 539–554. https://doi.org/10.5194/cp-15-539-2019

Barber, R. T., & Hiscock, M. R. (2006). A rising tide lifts all phytoplankton: Growth response of other phytoplankton taxa in diatom-dominated blooms. *Global Biogeochemical Cycles*, *20*(4). https://doi.org/10.1029/2006gb002726

Baumann, K.-H., Andruleit, H., Böckel, B., Geisen, M., & Kinkel, H. (2005). The significance of extant coccolithophores as indicators of ocean water masses, surface water temperature, and palaeoproductivity: A review. *Paläontologische Zeitschrift*, *79*, 93–112. https://doi.org/10.1007/bf03021756

Baumann, K.-H., & Freitag, T. (2004). Pleistocene fluctuations in the northern Benguela Current system as revealed by coccolith assemblages. *Marine Micropaleontology*, *52*, 195–215. https://doi.org/10.1016/j.marmicro.2004.04.011

Beaufort, L., Bolton, C., Sarr, A.-C., Suchéras-Marx, B., Rosenthal, Y., Donnadieu, Y., et al. (2020). *Cyclic evolution of phytoplankton forced by changes in tropical seasonality*.

Beaufort, L., Lancelot, Y., Camberlin, P., Cayre, O., Vincent, E., Bassinot, F., & Labeyrie, L. (1997). Insolation cycles as a major control of equatorial Indian Ocean primary production. *Science*, *278*, 1451–1454. https://doi.org/10.1126/science.278.5342.1451

Bendif, E. M., Nevado, B., Wong, E. L., Hagino, K., Probert, I., Young, J. R., et al. (2019). Repeated species radiations in the recent evolution of the key marine phytoplankton lineage Gephyrocapsa. *Nature Communications*, *10*, 1–9. https://doi.org/10.1038/s41467-019-12169-7

Benthien, A., Andersen, N., Schulte, S., Müller, P. J., Schneider, R. R., & Wefer, G. (2002). Carbon isotopic composition of the $C_{37:2}$ alkenone in core top sediments of the South Atlantic Ocean: Effects of CO_2 and nutrient concentrations. *Global Biogeochemical Cycles*, *16*, 11–12. https://doi.org/10.1029/2001gb001433

Bickert, T., Curry, W., & Wefer, G. (1997). Late Pliocene to Holocene (2.6–0 Ma) western equatorial Atlantic deep-water circulation: Inferences from benthic stable isotopes. In *Proceedings of the ocean drilling program. Scientific results* (pp. 239–253). https://doi.org/10.2973/odp.proc.sr.154.110.1997

Bidigare, R. R., Fluegge, A., Freeman, K. H., Hanson, K. L., Hayes, J. M., Hollander, D., et al. (1997). Consistent fractionation of ^{13}C in nature and in the laboratory: Growth-rate effects in some haptophyte algae. *Global Biogeochemical Cycles*, *11*, 279–292. https://doi.org/10.1029/96gb03939

Birch, H., Coxall, H. K., Pearson, P. N., Kroon, D., & O'Regan, M. (2013). Planktonic foraminifera stable isotopes and water column structure: Disentangling ecological signals. *Marine Micropaleontology*, *101*, 127–145. https://doi.org/10.1016/j.marmicro.2013.02.002

Blanco-Ameijeiras, S., Stoll, H. M., Zhang, H., & Hopkinson, B. M. (2020). Influence of temperature and CO_2 on plasma-membrane permeability to CO_2 and HCO_3^- in the marine haptophytes Emiliania huxleyi and Calcidiscus leptoporus (Prymnesiophyceae). *Journal of Phycology*. *56*(5).

Boller, A. J., Thomas, P. J., Cavanaugh, C. M., & Scott, K. M. (2011). Low stable carbon isotope fractionation by coccolithophore RubisCO. *Geochimica et Cosmochimica Acta*, *75*, 7200–7207. https://doi.org/10.1016/j.gca.2011.08.031

Boller, A. J., Thomas, P. J., Cavanaugh, C. M., & Scott, K. M. (2015). Isotopic discrimination and kinetic parameters of R ubis CO from the marine bloom-forming diatom, Skeletonema costatum. *Geobiology*, *13*, 33–43. https://doi.org/10.1111/gbi.12112

Bollmann, J., Baumann, K. H., & Thierstein, H. R. (1998). Global dominance of Gephyrocapsa coccoliths in the Late Pleistocene: Selective dissolution, evolution, or global environmental change? *Paleoceanography*, *13*, 517–529. https://doi.org/10.1029/98pa00610

Bolton, C. T., Hernández-Sánchez, M. T., Fuertes, M.-A., González-Lemos, S., Abrevaya, L., Mendez-Vicente, A., et al. (2016). Decrease in coccolithophore calcification and CO_2 since the middle Miocene. *Nature Communications*, *7*, 1–13. https://doi.org/10.1038/ncomms10284

Bolton, C. T., & Stoll, H. M. (2013). Late Miocene threshold response of marine algae to carbon dioxide limitation. *Nature*, *500*, 558–562. https://doi.org/10.1038/nature12448

Boyle, E., Edmond, J., & Sholkovitz, E. (1977). The mechanism of iron removal in estuaries. *Geochimica et Cosmochimica Acta*, *41*, 1313–1324. https://doi.org/10.1016/0016-7037(77)90075-8

Brassell, S., Brereton, R., Eglinton, G., Grimalt, J., Liebezeit, G., Marlowe, I., et al. (1986). Paleoclimatic signals recognized by chemometric treatment of molecular stratigraphic data. *Organic Geochemistry*, *10*, 649–660. https://doi.org/10.1016/s0146-6380(86)80001-8

Breitenbach, S. F., & Bernasconi, S. M. (2011). Carbon and oxygen isotope analysis of small carbonate samples (20 to 100 μg) with a GasBench II preparation device. *Rapid Communications in Mass Spectrometry*, *25*, 1910–1914. https://doi.org/10.1002/rcm.5052

Candelier, Y., Minoletti, F., Probert, I., & Hermoso, M. (2013). Temperature dependence of oxygen isotope fractionation in coccolith calcite: A culture and core top calibration of the genus Calcidiscus. *Geochimica et Cosmochimica Acta*, *100*, 264–281. https://doi.org/10.1016/j.gca.2012.09.040

Cassar, N., Laws, E. A., & Popp, B. N. (2006). Carbon isotopic fractionation by the marine diatom Phaeodactylum tricornutum under nutrient-and light-limited growth conditions. *Geochimica et Cosmochimica Acta*, *70*(21), 5323–5335. https://doi.org/10.1016/j.gca.2006.08.024

Cermeño, P., Lee, J.-B., Wyman, K., Schofield, O., & Falkowski, P. G. (2011). Competitive dynamics in two species of marine phytoplankton under non-equilibrium conditions. *Marine Ecology Progress Series*, *429*, 19–28. https://doi.org/10.3354/meps09088

Curry, W. B., Shackleton, N. J., Richter, C., & Party, S. S. (1995). Ocean drilling program. In *Proceedings of ODP, Initial Reports*. Citeseer.

Curry, W. B., Thunell, R. C., & Honjo, S. (1983). Seasonal changes in the isotopic composition of planktonic foraminifera collected in Panama Basin sediment traps. *Earth and Planetary Science Letters*, *64*(1), 33–43. https://doi.org/10.1016/0012-821x(83)90050-x

Dekens, P. S., Lea, D. W., Pak, D. K., & Spero, H. J. (2002). Core top calibration of Mg/Ca in tropical foraminifera: Refining paleotemperature estimation. *Geochemistry, Geophysics, Geosystems*, *3*, 1–29. https://doi.org/10.1029/2001gc000200

DeMaster, D. J., Kuehl, S. A., & Nittrouer, C. A. (1986). Effects of suspended sediments on geochemical processes near the mouth of the Amazon River: Examination of biological silica uptake and the fate of particle-reactive elements. *Continental Shelf Research*, *6*, 107–125. https://doi.org/10.1016/0278-4343(86)90056-7

Demaster, D. J., & Pope, R. H. (1996). Nutrient dynamics in Amazon shelf waters: Results from AMASSEDS. *Continental Shelf Research*, *16*, 263–289. https://doi.org/10.1016/0278-4343(95)00008-o

Dudley, W. C., Blackwelder, P., Brand, L., & Duplessy, J.-C. (1986). Stable isotopic composition of coccoliths. *Marine Micropaleontology*, *10*, 1–8. https://doi.org/10.1016/0377-8398(86)90021-6

Eppley, R. W., Rogers, J. N., & McCarthy, J. J. (1969). Half-saturation constants for uptake of nitrate and ammonium by marine phytoplankton. *Limnology & Oceanography*, *14*, 912–920. https://doi.org/10.4319/lo.1969.14.6.0912

Ezard, T. H., Edgar, K. M., & Hull, P. M. (2015). Environmental and biological controls on size-specific $\delta^{13}C$ and $\delta^{18}O$ in recent planktonic foraminifera. *Paleoceanography*, *30*, 151–173. https://doi.org/10.1002/2014pa002735

Flores, J., & Sierro, F. (1997). Revised technique for calculation of calcareous nannofossil accumulation rates. *Micropaleontology*, 321–324. https://doi.org/10.2307/1485832

Foster, G. L., Lear, C. H., & Rae, J. W. (2012). The evolution of pCO_2, ice volume and climate during the middle Miocene. *Earth and Planetary Science Letters*, *341*, 243–254. https://doi.org/10.1016/j.epsl.2012.06.007

Francois, R., & Bacon, M. P. (1991). Variations in terrigenous input into the deep equatorial Atlantic during the past 24,000 years. *Science*, *251*, 1473–1476. https://doi.org/10.1126/science.251.5000.1473

Fuertes, M.-Á., Flores, J.-A., & Sierro, F. J. (2014). The use of circularly polarized light for biometry, identification and estimation of mass of coccoliths. *Marine Micropaleontology*, *113*, 44–55. https://doi.org/10.1016/j.marmicro.2014.08.007

González Lemos, S., Guitián, J., Fuertes, M.-Á., Flores, J.-A., & Stoll, H. M. (2018). An empirical method for absolute calibration of coccolith thickness. *Biogeosciences*, *15*. https://doi.org/10.5194/bg-15-1079-2018

Guerreiro, C. V., Baumann, K.-H., Brummer, G.-J. A., Fischer, G., Korte, L. F., Merkel, U., et al. (2017). Coccolithophore fluxes in the open tropical North Atlantic: Influence of thermocline depth, Amazon water, and Saharan dust. *Biogeosciences*, *14*, 4577–4599. https://doi.org/10.5194/bg-14-4577-2017

Hastenrath, S., & Merle, J. (1987). Annual cycle of subsurface thermal structure in the tropical Atlantic Ocean. *Journal of Physical Oceanography*, *17*, 1518–1538. https://doi.org/10.1175/1520-0485(1987)017<1518:acosts>2.0.co;2

Henderiks, J., & Pagani, M. (2007). Refining ancient carbon dioxide estimates: Significance of coccolithophore cell size for alkenone-based pCO_2 records. *Paleoceanography*, *22*(3). PA3202. https://doi.org/10.1029/2006pa001399

Herbert, T., George, S. E., Marino, M., Maiorano, P., & Thunell, R. (2018). Alkenone-based approaches to productivity and growth rate. In AGU Fall Meeting (Vol. 2018, p. PP24B-02).

Herbert, T. D., Lawrence, K. T., Tzanova, A., Peterson, L. C., Caballero-Gill, R., & Kelly, C. S. (2016). Late Miocene global cooling and the rise of modern ecosystems. *Nature Geoscience*, *9*, 843–847. https://doi.org/10.1038/ngeo2813

Hermoso, M. (2015). Control of ambient pH on growth and stable isotopes in phytoplanktonic calcifying algae. *Paleoceanography*, *30*(8), 1100–1112. https://doi.org/10.1002/2015pa002844

Hermoso, M. (2016). Isotopic record of Pleistocene glacial/interglacial cycles in pelagic carbonates: Revisiting historical data from the Caribbean Sea. *Quaternary Science Reviews*, *137*, 69–78. https://doi.org/10.1016/j.quascirev.2016.02.003

Hermoso, M., Candelier, Y., Browning, T. J., & Minoletti, F. (2015). Environmental control of the isotopic composition of subfossil coccolith calcite: Are laboratory culture data transferable to the natural environment? *GeoResJ*, *7*, 35–42. https://doi.org/10.1016/j.grj.2015.05.002

Hermoso, M., Horner, T. J., Minoletti, F., & Rickaby, R. E. (2014). Constraints on the vital effect in coccolithophore and dinoflagellate calcite by oxygen isotopic modification of seawater. *Geochimica et Cosmochimica Acta*, *141*, 612–627. https://doi.org/10.1016/j.gca.2014.05.002

Hermoso, M., McClelland, H.-L. O., Hirst, J. S., Minoletti, F., Bonifacie, M., & Rickaby, R. E. M. (2020). Toward the use of the coccolith vital effects in paleoceanography: A field investigation during the middle Miocene in the SW Pacific Ocean. *Deep Sea Research Part I: Oceanographic Research Papers*, *160*, 103262. https://doi.org/10.1016/j.dsr.2020.103262

Hernández-Almeida, I., Ausín, B., Saavedra-Pellitero, M., Baumann, K.-H., & Stoll, H. M. (2019). Quantitative reconstruction of primary productivity in low latitudes during the last glacial maximum and the mid-to-late Holocene from a global Florisphaera profunda calibration dataset. *Quaternary Science Reviews*, *205*, 166–181. https://doi.org/10.1016/j.quascirev.2018.12.016

Hernández-Almeida, I., Krumhardt, K., Zhang, H., & Stoll, H. (2020). Estimation of physiological factors controlling carbon isotope fractionation in coccolithophores in photic zone and core-top samples. *Geochemistry, Geophysics, Geosystems*, *21*, e2020GC009272.

Holtz, L.-M., Wolf-Gladrow, D., & Thoms, S. (2017). Stable carbon isotope signals in particulate organic and inorganic carbon of coccolithophores—A numerical model study for Emiliania huxleyi. *Journal of Theoretical Biology*, *420*, 117–127. https://doi.org/10.1016/j.jtbi.2017.01.030

Hopkinson, B. M., Dupont, C. L., Allen, A. E., & Morel, F. M. (2011). Efficiency of the CO_2-concentrating mechanism of diatoms. *Proceedings of the National Academy of Sciences of the United States of America*, *108*(10), 3830–3837. https://doi.org/10.1073/pnas.1018062108

Jansen, J. H. F., Kuijpers, A., & Troelstra, S. R. (1986). A mid-Brunhes climatic event: Long-term changes in global atmosphere and ocean circulation. *Science*, *232*, 619–622. https://doi.org/10.1126/science.232.4750.619

Jasper, J. P., Hayes, J., Mix, A. C., & Prahl, F. G. (1994). Photosynthetic fractionation of ^{13}C and concentrations of dissolved CO_2 in the central equatorial Pacific during the last 255,000 years. *Paleoceanography*, *9*, 781–798. https://doi.org/10.1029/94pa02116

Jin, X., Liu, C., Zhang, H., Zhou, C., Jiang, X., Wu, Z., & Xu, J. (2018). Evolutionary driven of Gephyrocapsa coccolith isotopic vital effects over the past 400 ka. *Earth and Planetary Science Letters*, *503*, 236–247. https://doi.org/10.1016/j.epsl.2018.09.010

Key, R. M., Olsen, A., van Heuven, S., Lauvset, S. K., Velo, A., Lin, X., et al. (2015). *Global ocean data analysis project, version 2 (GLODAPv2), ORNL/CDIAC-162, ND-P093*, Carbon Dioxide Information Analysis Center, Oak Ridge National Laboratory, US Department of Energy.
Kinkel, H., Baumann, K.-H., & Cepek, M. (2000). Coccolithophores in the equatorial Atlantic Ocean: Response to seasonal and Late Quaternary surface water variability. *Marine Micropaleontology*, *39*, 87–112. https://doi.org/10.1016/s0377-8398(00)00016-5
Köhler, P., Nehrbass-Ahles, C., Schmitt, J., Stocker, T. F., & Fischer, H. (2017). A 156 kyr smoothed history of the atmospheric greenhouse gases CO_2, CH_4, and N_2O and their radiative forcing. *Earth System Science Data*, *9*, 363–387. https://doi.org/10.5194/essd-9-363-2017
Korte, L. F., Brummer, G. J. A., van der Does, M., Guerreiro, C. V., Mienis, F., Munday, C. I., et al. (2020). Multiple drivers of production and particle export in the western tropical North Atlantic. *Limnology & Oceanography*. *65*(9). https://doi.org/10.1002/lno.11442
Krumhardt, K. M., Lovenduski, N. S., Iglesias-Rodriguez, M. D., & Kleypas, J. A. (2017). Coccolithophore growth and calcification in a changing ocean. *Progress in Oceanography*, *159*, 276–295. https://doi.org/10.1016/j.pocean.2017.10.007
Lang, N., & Wolff, E. W. (2011). Interglacial and glacial variability from the last 800 ka in marine, ice and terrestrial archives. *Climate of the Past*, *7*(2), 361–380. https://doi.org/10.5194/cp-7-361-2011
Langer, G., Geisen, M., Baumann, K. H., Kläs, J., Riebesell, U., Thoms, S., & Young, J. R. (2006). Species-specific responses of calcifying algae to changing seawater carbonate chemistry. *Geochemistry, Geophysics, Geosystems*, *7*. Q09006. https://doi.org/10.1029/2005gc001227
Laws, E. A., Popp, B. N., Cassar, N., & Tanimoto, J. (2002). ^{13}C discrimination patterns in oceanic phytoplankton: Likely influence of CO_2 concentrating mechanisms, and implications for palaeoreconstructions. *Functional Plant Biology*, *29*(3), 323–333. https://doi.org/10.1071/pp01183
Leroy, L. (1939). Some small foraminifera, Ostracoda and otoliths from the Neogene of the Rokan-Tapanoeli area (central Sumatra). *Natuurkundig Tijdschrift voor Nederlandsch Indië*, *99*(6).
Lisiecki, L. E., & Stern, J. V. (2016). Regional and global benthic $\delta^{18}O$ stacks for the last glacial cycle. *Paleoceanography*, *31*, 1368–1394. https://doi.org/10.1002/2016pa003002
Liu, C., Cheng, X., Zhu, Y., Tian, J., & Xia, P. (2002). Oxygen and carbon isotope records of calcareous nannofossils for the past 1 Ma in the southern South China Sea. *Chinese Science Bulletin*, *47*, 798. https://doi.org/10.1360/02tb9180
Locarnini, R., Mishonov, A., Antonov, J., Boyer, T., Garcia, H., Baranova, O., et al. (2013). World Ocean Atlas 2013. In S. A. Levitus (Ed.), & Mishonov Technical (Eds.), *Temperature* (Vol. 73, p. 40). NOAA Atlas NESDIS.
Mann, K., & Lazier, J. (2006). *Vertical structure of the open ocean: Biology of the mixed layer: Dynamics of marine ecosystems*. Blackwell Publishing.
McClelland, H., Bruggeman, J., Hermoso, M., & Rickaby, R. (2017). The origin of carbon isotope vital effects in coccolith calcite. *Nature Communications*, *8*, 1–16. https://doi.org/10.1038/ncomms14511
Mejía, L. M., Méndez-Vicente, A., Abrevaya, L., Lawrence, K. T., Ladlow, C., Bolton, C., et al. (2017). A diatom record of CO_2 decline since the late Miocene. *Earth and Planetary Science Letters*, *479*, 18–33. https://doi.org/10.1016/j.epsl.2017.08.034
Mejía, L. M., Ziveri, P., Cagnetti, M., Bolton, C., Zahn, R., Marino, G., et al. (2014). Effects of midlatitude westerlies on the paleoproductivity at the Agulhas Bank slope during the penultimate glacial cycle: Evidence from coccolith Sr/Ca ratios. *Paleoceanography*, *29*, 697–714. https://doi.org/10.1002/2013pa002589
Molfino, B., & McIntyre, A. (1990). Precessional forcing of nutricline dynamics in the equatorial Atlantic. *Science*, *249*, 766–769. https://doi.org/10.1126/science.249.4970.766
Müller, P. J., Kirst, G., Ruhland, G., Von Storch, I., & Rosell-Melé, A. (1998). Calibration of the alkenone paleotemperature index U37K′ based on core-tops from the eastern South Atlantic and the global ocean (60°N-60°S). *Geochimica et Cosmochimica Acta*, *62*, 1757–1772. https://doi.org/10.1016/s0016-7037(98)00097-0
O'Dea, S. A., Gibbs, S. J., Bown, P. R., Young, J. R., Poulton, A. J., Newsam, C., & Wilson, P. A. (2014). Coccolithophore calcification response to past ocean acidification and climate change. *Nature Communications*, *5*, 1–7.
Okada, H., & Honjo, S. (1973). The distribution of oceanic coccolithophorids in the pacific,*Deep Sea Research and Oceanographic* (pp. 355–374). https://doi.org/10.1016/0011-7471(73)90059-4
Olsen, A., Key, R. M., van Heuven, S., Lauvset, S. K., Velo, A., Lin, X., et al. (2016). The Global Ocean Data Analysis Project version 2 (GLODAPv2)—An internally consistent data product for the world ocean. *Earth System Science Data*, *8*(2), 297–323. https://doi.org/10.5194/essd-8-297-2016
Orr, J., & Epitalon, J.-M. (2015). Improved routines to model the ocean carbonate system: Mocsy 2.0. (Vol. *8*). *Geoscientific Model Development*. https://doi.org/10.5194/gmd-8-485-2015
Pagani, M. (2014). 12.13 Biomarker-based inferences of past climate: The alkenone pCO_2 proxy. In H. D. Holland & K. K. Turekian (Eds.), *Treatise on geochemistry* (pp. 361–378). Elsevier. https://doi.org/10.1016/b978-0-08-095975-7.01027-5
Pagani, M., Freeman, K. H., & Arthur, M. A. (1999). Late Miocene atmospheric CO_2 concentrations and the expansion of C_4 grasses. *Science*, *285*, 876–879. https://doi.org/10.1126/science.285.5429.876
Pagani, M., Huber, M., Liu, Z., Bohaty, S. M., Henderiks, J., Sijp, W., et al. (2011). The role of carbon dioxide during the onset of Antarctic glaciation. *Science*, *334*, 1261–1264. https://doi.org/10.1126/science.1203909
Perrin, L., Probert, I., Langer, G., & Aloisi, G. (2016). Growth of the coccolithophore Emiliania huxleyi in light- and nutrient-limited batch reactors: Relevance for the BIOSOPE deep ecological niche of coccolithophores. *Biogeosciences*, *13*, 5983–6001. https://doi.org/10.5194/bg-13-5983-2016
Peterson, R. G., & Stramma, L. (1991). Upper-level circulation in the South Atlantic Ocean. *Progress in Oceanography*, *26*, 1–73. https://doi.org/10.1016/0079-6611(91)90006-8
Philander, S. (2001). *Atlantic Ocean equatorial currents*. Academic Press.
Philander, S., & Pacanowski, R. (1986). A model of the seasonal cycle in the tropical Atlantic Ocean. *Journal of Geophysical Research: Oceans*, *91*, 14192–14206. https://doi.org/10.1029/jc091ic12p14192
Popp, B. N., Laws, E. A., Bidigare, R. R., Dore, J. E., Hanson, K. L., & Wakeham, S. G. (1998). Effect of phytoplankton cell geometry on carbon isotopic fractionation. *Geochimica et Cosmochimica Acta*, *62*, 69–77. https://doi.org/10.1016/s0016-7037(97)00333-5
Prahl, F. G., & Wakeham, S. G. (1987). Calibration of unsaturation patterns in long-chain ketone compositions for paleotemperature assessment. *Nature*, *330*, 367–369. https://doi.org/10.1038/330367a0
Prell, W., & Curry, W. (1981). Faunal and isotopic indices of monsoonal upwelling—Western Arabian Sea. *Oceanologica Acta*, *4*, 91–98.
Rae, J. W., Zhang, Y. G., Liu, X., Foster, G. L., Stoll, H. M., & Whiteford, R. D. (2021). Atmospheric CO_2 over the past 66 million years from marine archives. *Annual Review of Earth and Planetary Sciences*, *49*. https://doi.org/10.1146/annurev-earth-082420-063026
Rau, G. H., Riebesell, U., & Wolf-Gladrow, D. (1996). A model of photosynthetic ^{13}C fractionation by marine phytoplankton based on diffusive molecular CO_2 uptake. *Marine Ecology Progress Series*, *133*, 275–285. https://doi.org/10.3354/meps133275

Ravelo, A., & Fairbanks, R. (1992). Oxygen isotopic composition of multiple species of planktonic foraminifera: Recorders of the modern photic zone temperature gradient. *Paleoceanography*, *7*, 815–831. https://doi.org/10.1029/92pa02092

R Core Team. (2021). *R: A language and environment for statistical computing*. R Foundation for Statistical Computing. Retrieved from http://www.R-project.org/

Rehfeld, K., Münch, T., Ho, S. L., & Laepple, T. (2018). Global patterns of declining temperature variability from the Last Glacial Maximum to the Holocene. *Nature*, *554*, 356–359. https://doi.org/10.1038/nature25454

Richardson, P., & Reverdin, G. (1987). Seasonal cycle of velocity in the Atlantic North Equatorial Countercurrent as measured by surface drifters, current meters, and ship drifts. *Journal of Geophysical Research*, *92*, 3691–3708. https://doi.org/10.1029/jc092ic04p03691

Rickaby, R. E., Henderiks, J., & Young, J. N. (2010). Perturbing phytoplankton: Response and isotopic fractionation with changing carbonate chemistry in two coccolithophore species. *Climate of the Past*, *6*, 771–785. https://doi.org/10.5194/cp-6-771-2010

Riegman, R., Stolte, W., Noordeloos, A. A. M., & Slezak, D. (2000). Nutrient uptake and alkaline phosphatase (ec 3:1:3:1) activity of emiliania huxleyi (PRYMNESIOPHYCEAE) during growth under n and p limitation in continuous cultures. *Journal of Phycology*, *36*, 87–96. https://doi.org/10.1046/j.1529-8817.2000.99023.x

Rigual-Hernández, A. S., Trull, T. W., Flores, J., Nodder, S. D., Eriksen, R., Davies, D. M., et al. (2020). Full annual monitoring of Subantarctic Emiliania huxleyi populations reveals highly calcified morphotypes in high-CO_2 winter conditions. *Scientific Reports*, *10*, 1–14. https://doi.org/10.1038/s41598-020-59375-8

Romanek, C. S., Grossman, E. L., & Morse, J. W. (1992). Carbon isotopic fractionation in synthetic aragonite and calcite: Effects of temperature and precipitation rate. *Geochimica et Cosmochimica Acta*, *56*, 419–430. https://doi.org/10.1016/0016-7037(92)90142-6

Schlitzer, R. (2008). *Ocean data view*.

Seki, O., Foster, G. L., Schmidt, D. N., Mackensen, A., Kawamura, K., & Pancost, R. D. (2010). Alkenone and boron-based Pliocene pCO_2 records. *Earth and Planetary Science Letters*, *292*, 201–211. https://doi.org/10.1016/j.epsl.2010.01.037

Sett, S., Bach, L. T., Schulz, K. G., Koch-Klavsen, S., Lebrato, M., & Riebesell, U. (2014). Temperature modulates coccolithophorid sensitivity of growth, photosynthesis and calcification to increasing seawater pCO_2. *PLoS One*, *9*, e88308. https://doi.org/10.1371/journal.pone.0088308

Sosdian, S. M., Greenop, R., Hain, M., Foster, G. L., Pearson, P. N., & Lear, C. H. (2018). Constraining the evolution of Neogene ocean carbonate chemistry using the boron isotope pH proxy. *Earth and Planetary Science Letters*, *498*, 362–376. https://doi.org/10.1016/j.epsl.2018.06.017

Spero, H. J., Mielke, K. M., Kalve, E. M., Lea, D. W., & Pak, D. K. (2003). Multispecies approach to reconstructing eastern equatorial Pacific thermocline hydrography during the past 360 kyr. *Paleoceanography*, *18*. 1022. https://doi.org/10.1029/2002pa000814

Steph, S., Regenberg, M., Tiedemann, R., Mulitza, S., & Nürnberg, D. (2009). Stable isotopes of planktonic foraminifera from tropical Atlantic/Caribbean core-tops: Implications for reconstructing upper ocean stratification. *Marine Micropaleontology*, *71*, 1–19. https://doi.org/10.1016/j.marmicro.2008.12.004

Stoll, H. M., Guitian, J., Hernandez-Almeida, I., Mejia, L. M., Phelps, S., Polissar, P., et al. (2019). Upregulation of phytoplankton carbon concentrating mechanisms during low CO_2 glacial periods and implications for the phytoplankton pCO_2 proxy. *Quaternary Science Reviews*, *208*, 1–20. https://doi.org/10.1016/j.quascirev.2019.01.012

Stolz, K., & Baumann, K.-H. (2010). Changes in paleoceanography and paleoecology during Marine Isotope Stage (MIS) 5 in the eastern North Atlantic (ODP Site 980) deduced from calcareous nannoplankton observations. *Palaeogeography, Palaeoclimatology, Palaeoecology*, *292*, 295–305. https://doi.org/10.1016/j.palaeo.2010.04.002

Stramma, L., & Schott, F. (1999). The mean flow field of the tropical Atlantic Ocean. *Deep Sea Research Part II: Topical Studies in Oceanography*, *46*, 279–303. https://doi.org/10.1016/s0967-0645(98)00109-x

Takahashi, T., Sutherland, S. C., Wanninkhof, R., Sweeney, C., Feely, R. a., Chipman, D. W., et al. (2009). Climatological mean and decadal change in surface ocean pCO_2, and net sea–air CO_2 flux over the global oceans. *Deep Sea Research Part II: Topical Studies in Oceanography*, *56*(8–10), 554–577. https://doi.org/10.1016/j.dsr2.2008.12.009

Tierney, J. E., & Tingley, M. P. (2018). BAYSPLINE: A new calibration for the alkenone paleothermometer. *Paleoceanography and Paleoclimatology*, *33*, 281–301. https://doi.org/10.1002/2017pa003201

Tremblin, M., Hermoso, M., & Minoletti, F. (2016). Equatorial heat accumulation as a long-term trigger of permanent Antarctic ice sheets during the Cenozoic. *Proceedings of the National Academy of Sciences of the United States of America*, *113*, 11782–11787. https://doi.org/10.1073/pnas.1608100113

Vink, A., Brune, A., Höll, C., Zonneveld, K. A., & Willems, H. (2002). On the response of calcareous dinoflagellates to oligotrophy and stratification of the upper water column in the equatorial Atlantic Ocean. *Palaeogeography, Palaeoclimatology, Palaeoecology*, *178*, 53–66. https://doi.org/10.1016/s0031-0182(01)00368-6

Volkman, J. K. (2000). Ecological and environmental factors affecting alkenone distributions in seawater and sediments. *Geochemistry, Geophysics, Geosystems*, *1*(9). 1036. https://doi.org/10.1029/2000gc000061

Waelbroeck, C., Kiefer, T., Dokken, T., Chen, M.-T., Spero, H., Jung, S., et al. (2014). Constraints on surface seawater oxygen isotope change between the Last Glacial Maximum and the Late Holocene. *Quaternary Science Reviews*, *105*, 102–111. https://doi.org/10.1016/j.quascirev.2014.09.020

Wilkens, R. H., Westerhold, T., Drury, A. J., Lyle, M., Gorgas, T., & Tian, J. (2017). Revisiting the Ceara Rise, equatorial Atlantic Ocean: Isotope stratigraphy of ODP Leg 154 from 0 to 5Ma. *Climate of the Past*, *13*, 779–793. https://doi.org/10.5194/cp-13-779-2017

Wilson, K. E., Maslin, M. A., & Burns, S. J. (2011). Evidence for a prolonged retroflection of the North Brazil Current during glacial stages. *Palaeogeography, Palaeoclimatology, Palaeoecology*, *301*, 86–96. https://doi.org/10.1016/j.palaeo.2011.01.003

Yin, Q. Z., & Berger, A. (2012). Individual contribution of insolation and CO_2 to the interglacial climates of the past 800,000 years. *Climate Dynamics*, *38*(3–4), 709–724. https://doi.org/10.1007/s00382-011-1013-5

Young, J., Geisen, M., Cros, L., Kleijne, A., Sprengel, C., Probert, I., & Østergaard, J. (2003). A guide to extant coccolithophore taxonomy. *Journal of Nannoplankton Research, Special Issue*, *1*, 1–132.

Young, J. R., Thierstein, H. R., & Winter, A. (2000). Nannoplankton ecology and paleoecology. *Marine Micropaleontology*, *1*(39), 7–9. https://doi.org/10.1016/s0377-8398(00)00009-8

Zeebe, R. E. (1999). An explanation of the effect of seawater carbonate concentration on foraminiferal oxygen isotopes. *Geochimica et Cosmochimica Acta*, *63*, 2001–2007. https://doi.org/10.1016/s0016-7037(99)00091-5

Zhang, H., Stoll, H., Bolton, C., Jin, X., & Liu, C. (2018). A refinement of coccolith separation methods: Measuring the sinking characteristics of coccoliths. *Biogeosciences*, *15*, 4759–4775. https://doi.org/10.5194/bg-15-4759-2018

Zhang, Y. G., Henderiks, J., & Liu, X. (2020). Refining the alkenone-pCO_2 method II: Toward resolving the physiological parameter '*b*'. *Geochimica et Cosmochimica Acta*, *281*, 118–134. https://doi.org/10.1016/j.gca.2020.05.002

Zhang, Y. G., Pagani, M., Liu, Z., Bohaty, S. M., & DeConto, R. (2013). A 40-million-year history of atmospheric CO_2. *Philosophical Transactions of the Royal Society A: Mathematical, Physical & Engineering Sciences*, *371*, 20130096. https://doi.org/10.1098/rsta.2013.0096

Ziveri, P., Stoll, H., Probert, I., Klaas, C., Geisen, M., Ganssen, G., & Young, J. (2003). Stable isotope 'vital effects' in coccolith calcite. *Earth and Planetary Science Letters*, *210*, 137–149. https://doi.org/10.1016/s0012-821x(03)00101-8

Ziveri, P., Thoms, S., Probert, I., Geisen, M., & Langer, G. (2012). A universal carbonate ion effect on stable oxygen isotope ratios in unicellular planktonic calcifying organisms. *Biogeosciences*, *9*, 1025–1032. https://doi.org/10.5194/bg-9-1025-2012

References From the Supporting Information

Bemis, B. E., Spero, H. J., Bijma, J., & Lea, D. W. (1998). Reevaluation of the oxygen isotopic composition of planktonic foraminifera: Experimental results and revised paleotemperature equations. *Paleoceanography*, *13*, 150–160. https://doi.org/10.1029/98pa00070

Boeckel, B., & Baumann, K.-H. (2004). Distribution of coccoliths in surface sediments of the south-eastern South Atlantic Ocean: Ecology, preservation and carbonate contribution. *Marine Micropaleontology*, *51*, 301–320. https://doi.org/10.1016/j.marmicro.2004.01.001

Bouvier-Soumagnac, Y., & Duplessy, J.-C. (1985). Carbon and oxygen isotopic composition of planktonic foraminifera from laboratory culture, plankton tows and Recent sediment; implications for the reconstruction of paleoclimatic conditions and of the global carbon cycle. *Journal of Foraminiferal Research*, *15*, 302–320. https://doi.org/10.2113/gsjfr.15.4.302

Buiteveld, H. (1995). A model for calculation of diffuse light attenuation (PAR) and Secchi depth. *Netherland Journal of Aquatic Ecology*, *29*(1), 55–65. https://doi.org/10.1007/bf02061789

Dittert, N., Baumann, K.-H., Bickert, R., Henrich, R., Huber, R., Kinkel, H., & Meggers, H. (1999). Carbonate dissolution in the deep-sea: Methods, quantification and paleoceanographic application. In G. Fischer & G. Wefer (Eds.), *Use of proxies in paleoceanography: Examples from the South Atlantic* (pp. 255–284). Springer Verlag. https://doi.org/10.1007/978-3-642-58646-0_10

Fielding, S. R. (2013). Emiliania huxleyi specific growth rate dependence on temperature. *Limnology & Oceanography*, *58*, 663–666. https://doi.org/10.4319/lo.2013.58.2.0663

Flores, J.-A., Gersonde, R., Sierro, F., & Niebler, H.-S. (2000). Southern Ocean Pleistocene calcareous nannofossil events: Calibration with isotope and geomagnetic stratigraphies. *Marine Micropaleontology*, *40*, 377–402. https://doi.org/10.1016/s0377-8398(00)00047-5

Flores, J. A., & Marino, M. (2002). Pleistocene calcareous nannofossil stratigraphy for ODP Leg 177 (Atlantic sector of the Southern Ocean). *Marine Micropaleontology*, *45*, 191–224. https://doi.org/10.1016/s0377-8398(02)00030-0

Hermoso, M., Minoletti, F., Aloisi, G., Bonifacie, M., McClelland, H. L. O., Labourdette, N., et al. (2016). An explanation for the ^{18}O excess in Noelaerhabdaceae coccolith calcite. *Geochimica et Cosmochimica Acta*, *189*, 132–142. https://doi.org/10.1016/j.gca.2016.06.016

Hoefs, J., & Hoefs, J. (2009). *Stable isotope geochemistry*. Springer.

Lin, J., Lee, Z., Ondrusek, M., & Du, K. (2016). Remote sensing of normalized diffuse attenuation coefficient of downwelling irradiance. *Journal of Geophysical Research: Oceans*, *121*(9), 6717–6730. https://doi.org/10.1002/2016jc011895

Murtugudde, R., Beauchamp, J., McClain, C. R., Lewis, M., & Busalacchi, A. J. (2002). Effects of penetrative radiation on the upper tropical ocean circulation. *Journal of Climate*, *15*(5), 470–486. https://doi.org/10.1175/1520-0442(2002)015<0470:eoprot>2.0.co;2

Regenberg, M., Steph, S., Nürnberg, D., Tiedemann, R., & Garbe-Schönberg, D. (2009). Calibrating Mg/Ca ratios of multiple planktonic foraminiferal species with $\delta^{18}O$-calcification temperatures: Paleothermometry for the upper water column. *Earth and Planetary Science Letters*, *278*(3–4), 324–336. https://doi.org/10.1016/j.epsl.2008.12.019